

Thermodynamics of classical one-dimensional generalized nonlinear Klein-Gordon lattice model

Hu-Wei Jia(贾虎伟), and Ning-Hua Tong(同宁华)
Citation: Chin. Phys. B, 2025, 34 (**8**): 080501. DOI: 10.1088/1674-1056/add50f
http://cpb.iphy.ac.cn; http://iopscience.iop.org/cpb

What follows is a list of articles you may be interested in

Optimal synchronization of higher-order Kuramoto model on hypergraphs

Chong-Yang Wang(王重阳), Bi-Yun Ji(季碧芸), and Linyuan Lü(吕琳媛)
Chin. Phys. B, 2025, 34 (**7**): 070502. DOI: 10.1088/1674-1056/adcded

Study and circuit design of stochastic resonance system based on memristor chaos induction

Qi Liang(梁琦), Wen-Xin Yu(于文新), and Qiu-Mei Xiao(肖求美)
Chin. Phys. B, 2025, 34 (**4**): 040502. DOI: 10.1088/1674-1056/adb268

Evaluating physical changes of iron oxide nanoparticles due to surface modification with oleic acid

S Rosales, N Casillas, A Topete, O Cervantes, G Gonz\'alez, J A Paz, and M E Cano†
Chin. Phys. B, 2020, 29 (**10**): 100502. DOI: 10.1088/1674-1056/aba2dc

Stochastic resonance in an under-damped bistable system driven by harmonic mixing signal

Yan-Fei Jin(靳艳飞)
Chin. Phys. B, 2018, 27 (**5**): 050501. DOI: 10.1088/1674-1056/27/5/050501

Rapidly calculating the partition function of macroscopic systems

Jing-Tian Li(李菁田), Bo-Yuan Ning(宁博元), Le-Cheng Gong(龚乐诚), Jun Zhuang(庄军), Xi-Jing Ning(宁西京)
Chin. Phys. B, 2017, 26 (**3**): 030501. DOI: 10.1088/1674-1056/26/3/030501

RAPID COMMUNICATION

Thermodynamics of classical one-dimensional generalized nonlinear Klein–Gordon lattice model

Hu-Wei Jia(贾虎伟)[1,2] and Ning-Hua Tong(同宁华)[1,2,†]

[1] *School of Physics, Renmin University of China, Beijing* 100872, *China*

[2] *Key Laboratory of Quantum State Construction and Manipulation (Ministry of Education), Renmin University of China, Beijing* 100872, *China*

(Received 15 April 2025; revised manuscript received 2 May 2025; accepted manuscript online 7 May 2025)

We study the thermodynamic properties of the classical one-dimensional generalized nonlinear Klein–Gordon lattice model ($n \geq 2$) by using the cluster variation method with linear response theory. The results of this method are exact in the thermodynamic limit. We present the single-site reduced density $\rho^{(1)}(z)$, averages such as $\langle z^2 \rangle$, $\langle |z^n| \rangle$, and $\langle (z_1 - z_2)^2 \rangle$, the specific heat C_v, and the static correlation functions. We analyze the scaling behavior of these quantities and obtain the exact scaling powers at the low and high temperatures. Using these results, we gauge the accuracy of the projective truncation approximation for the ϕ^4 lattice model.

Keywords: cluster variation method, linear response theory, one-dimensional generalized nonlinear Klein–Gordon lattice model

PACS: 05.20.Gg, 05.10.–a, 05.50.+q, 05.70.–a

DOI: 10.1088/1674-1056/add50f **CSTR:** 32038.14.CPB.add50f

1. Introduction

Many interesting phenomena in condensed matter physics are described by the classical many-body models. Examples include heat transport in a low-dimensional system,[1] glass transition,[2–4] anomalous attraction[5] and screening[6] in Coulomb fluid, condensation of DNA,[7,8] etc.

In order to study these phenomena with theoretical models, many statistical methods have been developed. On the numerical side, there are Monte Carlo (MC)[9] and molecular dynamics (MD) simulation[10,11] methods. On the analytical side, there are approaches such as variational approximations,[12–14] mode-coupling theory,[15,16] non-equilibrium Green's function,[17] projective truncation approximation (PTA) for Green's functions,[18,19] etc. But none of the above methods is exact.

Here, we focus on the classical one-dimensional generalized nonlinear Klein–Gordon (KG) lattice model.[20] It is an extension of the ϕ^4 lattice model[21] obtained from discretizing the continuous ϕ^4 field theory[22,23] to arbitrary potential index n. Both models are frequently used in the study of phonon properties and thermal transport of low-dimensional materials. Despite extensive numerical and analytical studies of the one-dimensional generalized nonlinear KG lattice model,[20] of which ϕ^4 is a special case, the exact thermodynamic properties of this model have not been addressed. In this work, we will fill this gap by combining the cluster variation method (CVM)[24] with the linear response theory (LRT).[25] Due to the exactness of this method for the one-dimensional lattice with nearest-neighbor coupling,[26–28] we are able to obtain the exact thermodynamic properties of this model in the thermodynamic limit.

We first give a brief review of CVM. CVM was first proposed by Kikuchi[24] to describe the order–disorder transition in the lattice gas model. In the modern form of this theory, the Peierls–Feynman–Bogoliubov variational free energy[29–31] is first formally expressed in terms of energy and entropy of the studied system. The entropy is then cumulant-expanded up to chosen clusters. Finally, the free energy is minimized with respect to the reduced density of the chosen cluster.[32,33] An[34] and Morita *et al.*[35] systematized the formalism and established general relations among quantities on sub-clusters and those on the largest chosen cluster, by using the concept of a partially ordered set and the Mobius inversion formula. Pelizzola[26–28] proved that CVM is exact for Ising-like models with discrete variables on (i) one-dimensional lattice and stripe system, (ii) tree-like lattice, (iii) (square) cactus lattice (the interior of Husmi tree), and (iv) square lattice with special coefficients. In particular, CVM based on nearest-neighbor two-site clusters is exact for models on the one-dimensional chain with nearest-neighbor interaction and open boundary condition.[36,37] The set of self-consistent CVM equations can be solved efficiently by the natural iteration method.[38–40] Unlike other cluster mean-field theories,[41,42] an important advantage of CVM is that the spatial translation symmetry of the original model is retained from the outset.

CVM has been widely applied in the study of clas-

†Corresponding author. E-mail: nhtong@ruc.edu.cn

© 2025 Chinese Physical Society and IOP Publishing Ltd. All rights, including for text and data mining, AI training, and similar technologies, are reserved.

sical and quantum lattice models. For classical systems, such studies include the order–disorder transition in Ising-like models,[24,43–47] the phase diagram of alloys[48,49] and multicomponent system.[50] For quantum systems, CVM has been employed to study the liquid helium,[32,33] Heisenberg model,[51,52] s–d model,[53] and the boson lattice gas.[54] For reviews, see Refs. [51,53,55]. Although originally developed and mostly applied to Ising-like models with discrete variables, CVM can be applied to study statistical models with continuous variables.[38,56,57] In this work, we will use CVM to study the one-dimensional generalized nonlinear KG lattice model which has continuous displacements on lattice sites.

In order to obtain the static spatial correlation function beyond the size of the chosen cluster (nearest-neighbor pairs in this work), we combine CVM with LRT. In CVM, LRT has been used to calculate correlation functions in Refs. [35,44,45,47]. LRT has also been used in the closely related belief propagation to do probabilistic inference via massive probabilistic model.[58,59] Note that our LRT here refers to the linear response to static external fields only.

This paper is arranged as follows. In Section 2, we introduce the one-dimensional generalized nonlinear KG lattice model and its scaling properties. In Section 3, we present the formulation of CVM and LRT. In Section 4, the numerical data are shown and physical results are analyzed. In particular, in Subsection 4.5, we compare CVM results with those from PTA[18] for the ϕ^4 model. Section 5 gives a summary and discussion.

2. The classical one-dimensional generalized nonlinear KG lattice model

The Hamiltonian of the generalized nonlinear KG model studied in this work reads

$$H(K,\gamma)=\sum_{i=1}^{L}\frac{p_i^2}{2m}+\sum_{i=1}^{L}\frac{K}{2}\left(x_i-x_{i+1}\right)^2+\sum_{i=1}^{L}\frac{\gamma}{n}\left|x_i\right|^n. \quad (1)$$

The dynamical variables x_i and p_i are the displacement from the equilibrium position and the momentum of atom i ($1\le i\le L$), respectively. L is the total number of atoms along the chain. n is the exponent of the on-site potential. K and γ are the strengths of the nearest-neighbor coupling and local potential, respectively. We impose the periodic boundary condition $x_{L+1}=x_1$ and $p_{L+1}=p_1$. In this work we set $m=1$.

The generalized nonlinear KG lattice model presented above is a generalization of the ϕ^4 lattice model by extending the exponent 4 of the local potential to an arbitrary value $n>0$. The ϕ^4 lattice model is obtained by discretizing the field theoretical KG model[60,61] with the added nonlinear local term ϕ^4. It is widely used in the study of heat transport in low dimensional systems.[17,23,62,63] By extending the index from 4 to n, the shape of the local potential well can be tuned from a very weak confinement ($n\sim 0$)[64] to the infinite square well ($n=\infty$). The competition between the local and the nonlocal interactions varies in this process. This model therefore has a richer behavior of physical quantities and has been used as a toy model for studying the influence of nonlinear interaction on lattice dynamics and thermal transport.[20] Below, we will denote this model as the KG lattice model.

Previous studies of this model mostly focused on the $n=4$ case, i.e., ϕ^4 model. On the side of dynamical properties, MD simulations[62,63] and non-equilibrium Green's function method[17] have been used to study the phonon dispersion and the relaxation. A normal thermal transport has been found,[23] with a power law temperature dependence of thermal conductivity as $\kappa\sim T^{-1.35}$ for $n=4$. For cases of $1<n<2$ and $n>2$, the phenomenological effective phonon theory gives $\kappa\sim T^{4(2-n)/(n+2)}$.[20,64] On the side of thermodynamic properties, for ϕ^4 field theory ($n=4$), quantities such as the average energy, $\langle x^2\rangle$, and correlation function have been calculated by mapping the classical statistical problem into a trace for the one-dimensional quantum anharmonic oscillator.[22] Low and high temperature asymptotic power laws are obtained with numerically exact coefficients. For general n, MD simulations confirm that the low temperature power laws $\langle x^2\rangle\sim T^{4/(n+2)}$ and $\langle|x|^n\rangle\sim T^{2n/(n+2)}$ from the Hartree–Fock approximation are valid.[20] For other quantities such as the specific heat and correlation function, a systematic study has not been carried out.

Like the ϕ^4 lattice model and FPU model,[10] the KG lattice model with general parameter n has the following scaling properties:[23,65]

$$H(K,\gamma)=g\tilde{H}(1,1). \quad (2)$$

Here,

$$\tilde{H}(K,\gamma)=\sum_{i=1}^{L}\frac{\tilde{p}_i^2}{2m}+\sum_{i=1}^{L}\frac{K}{2}\left(\tilde{x}_i-\tilde{x}_{i+1}\right)^2+\sum_{i=1}^{L}\frac{\gamma}{n}\left|\tilde{x}_i\right|^n, \quad (3)$$

$$g=\left(\frac{K^n}{\gamma^2}\right)^{\frac{1}{n-2}}. \quad (4)$$

The rescaled variables $\tilde{x}_i$ and $\tilde{p}_i$ are related to the original ones by

$$p_i=\sqrt{K}\left(\frac{K}{\gamma}\right)^{\frac{1}{n-2}}\tilde{p}_i,\ \ x_i=\left(\frac{K}{\gamma}\right)^{\frac{1}{n-2}}\tilde{x}_i. \quad (5)$$

Note that the above transformation does not conserve the Poisson bracket. But for the statistical properties that can be calculated from the integration of variables only, the above transformation is useful in that the results for the Hamiltonian $H(K,\gamma)$ in Eq. (1) at arbitrary parameter (K,γ) can be recovered from those for $H(K=1,\gamma=1)$ using the scaling relations. For example, we have

$$\langle|x|^m\rangle(K,\gamma,T)=\left(\frac{K}{\gamma}\right)^{\frac{m}{n-2}}\langle|x|^m\rangle\left(1,1,g^{-1}T\right), \quad (6)$$

$$C_{\rm v}(K,\gamma,T) = gC_{\rm v}\left(1,1,g^{-1}T\right), \tag{7}$$

$$\xi(K,\gamma,T) = \xi\left(1,1,g^{-1}T\right). \tag{8}$$

Therefore, in this paper, we only study the Hamiltonian $H(K=1,\gamma=1)$. For convenience, we write it as a sum of three parts

$$H(K=1,\gamma=1) = \sum_{i=1}^{L}\left[E_k(p_i)+U(x_i)+V(x_i,x_{i+1})\right], \tag{9}$$

with

$$E_k(p) = \frac{p^2}{2m},\ \ U(x) = \frac{1}{n}|x|^n,\ \ V(x,y) = \frac{1}{2}(x-y)^2. \tag{10}$$

Here, $E_k(p)$ is the kinetic energy, $U(x)$ is the local potential, and $V(x,y)$ is the nearest-neighbor coupling. This form of Hamiltonian will be used in the derivation and computation below.

3. Formula of CVM and LRT

In this section, we present the detailed derivation of CVM and LRT formula for Hamiltonian (9).

3.1. CVM formula

For the sake of completeness, in this part we first summarize the basic formalism of CVM. Then we apply it to the one-dimensional KG lattice model Eq. (9). We start from the minimization principle of free energy F,

$$F \leqslant F[\rho(\boldsymbol{p},\boldsymbol{x})] \equiv \langle H\rangle_\rho + k_{\rm B}T\langle\ln\rho(\boldsymbol{p},\boldsymbol{x})\rangle_\rho. \tag{11}$$

Here F and H are the free energy and Hamiltonian of the studied system, respectively. $\rho = \rho(\boldsymbol{p},\boldsymbol{x})$ is the density operator (where $\boldsymbol{p} = \{p_1,p_2,\ldots,p_L\}$ and $\boldsymbol{q} = \{q_1,q_2,\ldots,q_L\}$). Thermodynamic average $\langle O\rangle_\rho$ is defined as $\langle O\rangle_\rho = \iint O(\boldsymbol{p},\boldsymbol{x})\rho(\boldsymbol{p},\boldsymbol{x})\mathrm{d}\boldsymbol{p}\mathrm{d}\boldsymbol{x}/\iint\rho(\boldsymbol{p},\boldsymbol{x})\mathrm{d}\boldsymbol{p}\mathrm{d}\boldsymbol{x}$. Minimizing the functional $F[\rho(\boldsymbol{p},\boldsymbol{x})]$ with respect to $\rho(\boldsymbol{p},\boldsymbol{x})$ under the constraint $\iint\rho(\boldsymbol{p},\boldsymbol{x})\mathrm{d}\boldsymbol{p}\mathrm{d}\boldsymbol{x}=1$ will give the density operator $\rho_{\rm eq}(\boldsymbol{p},\boldsymbol{x}) = \mathrm{e}^{-\beta H}/\iint\mathrm{e}^{-\beta H}\mathrm{d}\boldsymbol{p}\mathrm{d}\boldsymbol{x}$ and free energy F of the equilibrium state. Here $\beta = 1/(k_{\rm B}T)$, with $k_{\rm B}$ being the Boltzmann constant and T the absolute temperature. Below, we will work under the natural unit $k_{\rm B}=1$.

CVM is based on minimizing F with respect to the reduced density operators of a chosen set of clusters. To do this, one first chooses a set of basic, mutually non-inclusive clusters. Then one approximately expresses the free energy functional $F[\rho(\boldsymbol{p},\boldsymbol{x})]$ in terms of the reduced density operators $\rho_c(\boldsymbol{p}_c,\boldsymbol{x}_c)$ (where $\boldsymbol{p}_c = \{p_1,p_2,\ldots,p_{|c|}\}$ and $\boldsymbol{x}_c = \{x_1,x_2,\ldots,x_{|c|}\}$, $|c|$ denotes the number of lattice sites in cluster c) of the basic clusters and their sub-clusters. For the short-range interacting system with Hamiltonian $H = \sum_c H_c$, we suppose the average energy $\langle H\rangle = \sum_c\langle H_c\rangle_{\rho_c} = \sum_c\int\mathrm{d}\boldsymbol{p}_c\mathrm{d}\boldsymbol{x}_c\rho_c(\boldsymbol{p}_c,\boldsymbol{x}_c)H_c(\boldsymbol{p}_c,\boldsymbol{x}_c)$ can already be expressed as a functional of the cluster density operators ρ_c. One can express the negative entropy of an L-site system $-S_L = \langle\ln\rho\rangle_\rho$ in terms of cluster quantities through the cumulant expansion

$$-S_L \equiv \Gamma_L = \sum_i^L\gamma_i^{(1)} + \sum_{i<j}^L\gamma_{ij}^{(2)} + \sum_{i<j<k}^L\gamma_{ijk}^{(3)} + \cdots. \tag{12}$$

In the above equation, $\gamma^{(n)}_{i_1,i_2,\ldots,i_n}$ $(n=1,2,\ldots,L)$ is the cumulant entropy of the n-site cluster composed of sites $(i_1,i_2,\ldots,i_n)$.

In CVM, the above expansion is truncated to the chosen set of basic clusters and their sub-clusters, under the assumption that the neglected terms are sufficiently small. For each cluster c appearing in the truncated expansion, its entropy S_c is related to the cumulant entropies of its sub-clusters (including itself) via a similar expression

$$-S_c \equiv \Gamma_c = \sum_i^c\gamma_i^{(1)} + \sum_{i<j}^c\gamma_{ij}^{(2)} + \sum_{i<j<k}^c\gamma_{ijk}^{(3)} + \cdots. \tag{13}$$

Here the expansion runs over all sub-clusters of c, including the cluster c itself. This equation can be written down for every sub-cluster of c, generating a closed set of linear equations for all the involved cumulant entropies $\gamma^{(n)}_{i_1,i_2,\ldots,i_n}$ $(n=1,2,\ldots,|c|)$. By the Möbius inversion, the linear equations can be solved to express the cumulant entropies γ's in terms of $\Gamma_{c'}$'s of clusters $c'\subseteq c$ which can be explicitly written as functionals of the cluster density operators $\rho_{c'}$

$$\Gamma_{c'} = \langle\ln\rho_{c'}\rangle_{\rho_{c'}}. \tag{14}$$

Putting γ's back into Eq. (12), one finally expresses $-S_L$ as functional of cluster density operators. The variation of free energy $F[\rho]$ in Eq. (11) is then carried out with respect to all the involved ρ_c, under the constraints

$$\begin{aligned}&\int\rho_c(\boldsymbol{p}_c,\boldsymbol{x}_c)\mathrm{d}\boldsymbol{p}_c\mathrm{d}\boldsymbol{x}_c = 1;\\ &\int\rho_c(\boldsymbol{p}_c,\boldsymbol{x}_c)\mathrm{d}\boldsymbol{p}_{c-c'}\mathrm{d}\boldsymbol{x}_{c-c'} = \rho_{c'}(\boldsymbol{p}_{c'},\boldsymbol{x}_{c'}),\ \ (\forall c'\subset c).\end{aligned} \tag{15}$$

In the second line of Eq. (15), the integral symbol $\int\mathrm{d}\boldsymbol{p}_{c-c'}\mathrm{d}\boldsymbol{x}_{c-c'}$ represents the integration of degrees of freedom in cluster c but outside cluster $c'\subset c$.

To apply CVM to Hamiltonian Eq. (9), we first separate the total free energy F into the kinetic part $F_{\rm kin}$ and the potential energy part $F_{\rm pot}$,

$$\begin{aligned}&F = F_{\rm kin} + F_{\rm pot},\\ &F_{\rm kin} = -\frac{1}{\beta}\ln\left[\prod_{i=1}^L\int_{-\infty}^{+\infty}\mathrm{d}p_i\,\mathrm{e}^{-\beta E_{\rm k}(p_i)}\right],\\ &F_{\rm pot} = -\frac{1}{\beta}\ln\left[\int\cdots\int_{-\infty}^{+\infty}\prod_{i=1}^L\mathrm{d}x_i\,\mathrm{e}^{-\beta\sum_{i=1}^L[U(x_i)+V(x_i,x_{i+1})]}\right].\end{aligned} \tag{16}$$

Only the potential energy part $F_{\rm pot}$ needs to be treated by CVM. Therefore, in the rest of the paper, we will use H, F,

and S_L to refer to the potential energy part of the corresponding quantities. The kinetic contribution to the total free energy will be added whenever necessary.

For the one-dimensional model with nearest-neighbor coupling, our basic cluster set is composed of all the nearest-neighbor pairs. It not only covers all the interaction terms in the Hamiltonian, but also is the minimum set that supports the exact cumulant expansion of S_L for the one-dimensional chain with an open boundary condition. This is because the joint density distribution $\rho^{(L)}(x_1,x_2,\ldots,x_L)$ for our L-site KG lattice model with open boundary condition can be exactly expressed as[28]

$$\begin{aligned}&\rho^{(L)}(x_1,x_2,\ldots,x_L)\\&=\frac{\rho_{12}^{(2)}(x_1,x_2)\rho_{23}^{(2)}(x_2,x_3)\cdots\rho_{L-1,L}^{(2)}(x_{L-1},x_L)}{\rho_2^{(1)}(x_2)\rho_3^{(1)}(x_3)\cdots\rho_{L-1}^{(1)}(x_{L-1})}.\end{aligned}\tag{17}$$

Here, $\rho_i^{(1)}(x_i)$ and $\rho_{i,i+1}^{(2)}(x_i,x_{i+1})$ are the reduced densities of site i and pair $(i,i+1)$, respectively. As a consequence, the cumulant expansion of entropy in Eq. (12) terminates rigorously at second order.

Since our Hamiltonian (1) is defined with a periodic boundary condition, CVM based on neighbor-neighbor pairs is not exact for this Hamiltonian with finite chain length L. In the limit $L=\infty$, however, the open and periodic boundary conditions are equivalent for this system. As we will see below (Eq. (31)), under the lattice translation invariance of Eq. (1), our CVM equations do not contain L. They can therefore be applied directly to $L=\infty$ to produce exact results for the thermodynamic limit.

With this choice of basic clusters, the average energy (interaction part only) reads

$$\langle H\rangle=\sum_{i=1}^{L}\left[\langle U(x_i)\rangle+\langle V(x_i,x_{i+1})\rangle\right],\tag{18}$$

with

$$\begin{aligned}\langle U(x_i)\rangle&=\int_{-\infty}^{+\infty}\mathrm{d}x\rho_i^{(1)}(x)U(x),\\\langle V(x_i,x_{i+1})\rangle&=\iint_{-\infty}^{+\infty}\mathrm{d}x\mathrm{d}y\,\rho_{i,i+1}^{(2)}(x,y)V(x,y).\end{aligned}\tag{19}$$

Functions $U(x)$ and $V(x,y)$ are given in Eq. (10). The entropy term is obtained as

$$\begin{aligned}-S_L\equiv\Gamma_L&=\sum_{i=1}^{L}\gamma_i^{(1)}+\sum_{i=1}^{L}\gamma_{i,i+1}^{(2)}\\&=\sum_{i=1}^{L}\Gamma_i^{(1)}+\sum_{i=1}^{L}\left[\Gamma_{i,i+1}^{(2)}-\Gamma_i^{(1)}-\Gamma_{i+1}^{(1)}\right].\end{aligned}\tag{20}$$

Here, $\Gamma_i^{(1)}$ and $\Gamma_{i,i+1}^{(2)}$ are the negative entropies of single-site and nearest-neighbor pair, respectively,

$$\begin{aligned}\Gamma_i^{(1)}&=\int_{-\infty}^{+\infty}\mathrm{d}x\rho_i^{(1)}(x)\ln\rho_i^{(1)}(x),\\\Gamma_{i,i+1}^{(2)}&=\iint_{-\infty}^{+\infty}\mathrm{d}x\mathrm{d}y\,\rho_{i,i+1}^{(2)}(x,y)\ln\rho_{i,i+1}^{(2)}(x,y).\end{aligned}\tag{21}$$

Considering the spatial translation invariance, we obtain the final expression for F/L as

$$F/L=\langle U(x)\rangle+\langle V(x,y)\rangle+T\left[\Gamma^{(2)}-\Gamma^{(1)}\right].\tag{22}$$

The averages are readily expressed in terms of $\rho^{(1)}(x)$ and $\rho^{(2)}(x,y)$ as

$$\begin{aligned}\langle U(x)\rangle&=\frac{1}{n}\int_{-\infty}^{+\infty}\mathrm{d}x\rho^{(1)}(x)\,|x|^n,\\\langle V(x,y)\rangle&=\frac{1}{2}\iint_{-\infty}^{+\infty}\mathrm{d}x\mathrm{d}y\,\rho^{(2)}(x,y)(x-y)^2.\end{aligned}\tag{23}$$

The last two terms in Eq. (22) read

$$\begin{aligned}\Gamma^{(1)}&=\int_{-\infty}^{+\infty}\mathrm{d}x\rho^{(1)}(x)\ln\rho^{(1)}(x),\\\Gamma^{(2)}&=\iint_{-\infty}^{+\infty}\mathrm{d}x\mathrm{d}y\,\rho^{(2)}(x,y)\ln\rho^{(2)}(x,y).\end{aligned}\tag{24}$$

Equations (22)–(24) give the explicit expression for the functional $F[\rho^{(1)},\rho^{(2)}]$.

The variation of $F[\rho^{(1)},\rho^{(2)}]$ must be carried out under the following normalization and reducibility constraints:

$$\begin{aligned}&\int_{-\infty}^{+\infty}\mathrm{d}x\rho^{(1)}(x)=1,\quad\int_{-\infty}^{+\infty}\mathrm{d}y\rho^{(2)}(x,y)=\rho^{(1)}(x),\\&\int_{-\infty}^{+\infty}\mathrm{d}x\rho^{(2)}(x,y)=\rho^{(1)}(y),\quad\iint_{-\infty}^{+\infty}\mathrm{d}x\mathrm{d}y\rho^{(2)}(x,y)=1.\end{aligned}\tag{25}$$

Enforcing the four constraints by Lagrangian multipliers λ_1, $\lambda_2(x)$, $\lambda_3(x)$, and λ_4, respectively, we obtain the functional to be varied as

$$\begin{aligned}\tilde{F}/L=\;&F/L-\lambda_1\left[\int_{-\infty}^{+\infty}\mathrm{d}x\rho^{(1)}(x)-1\right]\\&-\int_{-\infty}^{+\infty}\mathrm{d}x\lambda_2(x)\left[\int_{-\infty}^{+\infty}\mathrm{d}y\rho^{(2)}(x,y)-\rho^{(1)}(x)\right]\\&-\int_{-\infty}^{+\infty}\mathrm{d}y\lambda_3(y)\left[\int_{-\infty}^{+\infty}\mathrm{d}x\rho^{(2)}(x,y)-\rho^{(1)}(y)\right]\\&-\lambda_4\left[\iint_{-\infty}^{+\infty}\mathrm{d}x\mathrm{d}y\,\rho^{(2)}(x,y)-1\right].\end{aligned}\tag{26}$$

Carrying out the functional derivative of $\tilde{F}/L$ with respect to λ_1, $\lambda_2(z)$, $\lambda_3(z)$, and λ_4 gives the four constraints Eq. (25), while with respect to $\rho^{(1)}(z)$ and $\rho^{(2)}(z,w)$ gives

$$\rho^{(1)}(z)=\mathrm{e}^{\beta[U(z)+\lambda_2(z)+\lambda_3(z)-\lambda_1]-1},\tag{27}$$

$$\rho^{(2)}(z,w)=\mathrm{e}^{\beta[-V(z,w)+\lambda_2(z)+\lambda_3(w)+\lambda_4]-1}.\tag{28}$$

For the case of symmetric coupling $V(x-y)=V(y-x)$ studied in this paper (see Eq. (10)), we can prove that $\lambda_2(z)=$

$\lambda_3(z)$, which can be determined only up to an additive constant. Therefore, the one-site reduced density $\rho^{(1)}(z)$ can be rewritten as

$$\rho^{(1)}(z) = \mathrm{e}^{\beta[U(z)+2\lambda_2(z)-\lambda_1]-1}. \tag{29}$$

Similarly, $\rho^{(2)}(z,w)$ is given by

$$\rho^{(2)}(z,w) = \mathrm{e}^{\beta[-V(z,w)+\lambda_2(z)+\lambda_2(w)+\lambda_4]-1}. \tag{30}$$

Substituting Eqs. (29) and (30) into Eq. (25), the self-consistent equations about $\lambda_1+\lambda_4$ and $\lambda_2(z)$ are finally reduced to the following form:

$$\begin{aligned}
&\mathrm{e}^{\beta(\lambda_1+\lambda_4)} = \frac{\int_{-\infty}^{+\infty}\mathrm{d}z\,\mathrm{e}^{\beta[U(z)+2\lambda_2(z)]}}{\int_{-\infty}^{+\infty}\mathrm{d}z\,\mathrm{e}^{\beta[Q(z)+\lambda_2(z)]}},\\
&\lambda_2(z) = Q(z) - U(z) + \lambda_1 + \lambda_4,\\
&\mathrm{e}^{\beta Q(z)} = \int_{-\infty}^{+\infty}\mathrm{d}w\,\mathrm{e}^{\beta[\lambda_2(w)-V(z,w)]}.
\end{aligned} \tag{31}$$

If we insert $\lambda_2(z)=\lambda_3(z)$ into Eqs. (29) and (30), and compare them with $\mathrm{e}^{-\beta H_i}$ and $\mathrm{e}^{-\beta H_{i,i+1}}$, we see that $Q(z)$ describes the influence of the rest of the chain sites on the one-site and two-site clusters. Here the formalism is exact, but in general cases it plays the role of a mean field exerted on the clusters.

The above formula of CVM for one-dimensional KG lattice model does not contain the system size L and hence applies to arbitrary size, in particular, $L=\infty$. In this limit, the periodic boundary condition used in our Hamiltonian is equivalent to the open boundary condition for which the two-site CVM is exact. The numerical confirmation of this issue is presented in Fig. 7.

Note that unlike the conventional cluster extension of the Weiss mean-field theories, under certain situations, CVM can preserve the correlation beyond the cluster size due to a clever imbedding of the cluster into the full system. For the one-dimensional KG lattice model with nearest-neighbor coupling and open boundary condition, a two-site cluster is the minimum unit that can preserve all the nonlocal correlations in CVM. In the CVM with one-site cluster, the nonlocal correlation will be truncated, leading to decoupled oscillators. The results are valid only in the high temperature limit. The Bethe–Peierls approximation is equivalent to the two-site CVM and it will give exact results for our one-dimensional system with open boundary condition.[26]

3.2. Linear response theory

The above CVM formalism only produces $\rho^{(1)}(z)$ and $\rho^{(2)}(z,w)$, which contain local and nearest-neighbor correlations. In order to obtain the long-range correlation functions such as $\langle x_i x_j\rangle$ for arbitrary i and j, we resort to the linear response theory.

We add the following local external field terms to the original Hamiltonian (10):

$$H' = -\sum_{i=1}^{L} h_i B(x_i). \tag{32}$$

Here h_i is the local field on site i and $B(x_i)$ is a function of x_i, to be specified below. The total Hamiltonian at $K=1$ and $\gamma=1$ becomes

$$H = \sum_{i=1}^{L}\frac{p_i^2}{2m} + \sum_{i=1}^{L}\frac{1}{n}|x_i|^n + \sum_{i=1}^{L}\frac{1}{2}(x_i - x_{i+1})^2 + H'. \tag{33}$$

Applying the nearest-neighbor pair CVM to the above H, we obtain the variational free energy (interaction part)

$$\begin{aligned}
F \;=\; &\sum_{i=1}^{L}\langle U(x_i)\rangle + \sum_{i=1}^{L}\langle V(x_i,x_{i+1})\rangle - \sum_{i=1}^{L} h_i\langle B(x_i)\rangle\\
&+T\sum_{i}^{L}\left[\Gamma_{i,i+1}^{(2)} - \Gamma_i^{(1)}\right].
\end{aligned} \tag{34}$$

Here, $\langle U(x_i)\rangle$, $\langle V(x_i,x_{i+1})\rangle$ are given by Eq. (19) and $\Gamma_i^{(1)}$, $\Gamma_{i,i+1}^{(2)}$ by Eq. (21).

In the above equation, $\rho_i^{(1)}(x)$ and $\rho_{i,i+1}^{(2)}(x,y)$ obey the following constraints:

$$\begin{aligned}
&\int_{-\infty}^{+\infty}\mathrm{d}x\rho_i^{(1)}(x) = 1,\quad \int_{-\infty}^{+\infty}\mathrm{d}y\rho_{i,i+1}^{(2)}(x,y) = \rho_i^{(1)}(x),\\
&\int_{-\infty}^{+\infty}\mathrm{d}x\rho_{i,i+1}^{(2)}(x,y) = \rho_{i+1}^{(1)}(y),\\
&\iint_{-\infty}^{+\infty}\mathrm{d}x\mathrm{d}y\,\rho_{i,i+1}^{(2)}(x,y) = 1.
\end{aligned} \tag{35}$$

They are enforced by Lagrangian multipliers λ_{1i}, $\lambda_{2i}(z)$, $\lambda_{3i}(z)$, and λ_{4i}, respectively. We get

$$\begin{aligned}
\tilde{F} \;=\; &F - \sum_{i=1}^{L}\lambda_{1i}\left[\int_{-\infty}^{+\infty}\mathrm{d}x\rho_i^{(1)}(x) - 1\right]\\
&-\sum_{i=1}^{L}\int_{-\infty}^{+\infty}\mathrm{d}x\lambda_{2i}(x)\left[\int_{-\infty}^{+\infty}\mathrm{d}y\rho_{i,i+1}^{(2)}(x,y) - \rho_i^{(1)}(x)\right]\\
&-\sum_{i=1}^{L}\int_{-\infty}^{+\infty}\mathrm{d}y\lambda_{3i+1}(y)\left[\int_{-\infty}^{+\infty}\mathrm{d}x\rho_{i,i+1}^{(2)}(x,y) - \rho_{i+1}^{(1)}(y)\right]\\
&-\sum_{i=1}\lambda_{4i}\left[\iint_{-\infty}^{+\infty}\mathrm{d}x\mathrm{d}y\rho_{i,i+1}^{(2)}(x,y) - 1\right].
\end{aligned} \tag{36}$$

Carrying out the variation of $\tilde{F}$ with respect to λ_{1i}, $\lambda_{2i}(z)$, $\lambda_{3i}(z)$, and λ_{4i} will produce the constraint equation (35). The variation with respect to $\rho_i^{(1)}(z)$ and $\rho_{i,i+1}^{(2)}(z,w)$ then gives

$$\rho_i^{(1)}(z) = \mathrm{e}^{\beta[U(z)-h_iB(z)+\lambda_{2i}(z)+\lambda_{3i}(z)-\lambda_{1i}]-1}, \tag{37}$$

$$\rho_{i,i+1}^{(2)}(z,w) = \mathrm{e}^{\beta[-V(z,w)+\lambda_{2i}(z)+\lambda_{3i+1}(w)+\lambda_{4i}]-1}. \tag{38}$$

In the limit $\{h_i\}=0$, the above equations reduce to the uniform CVM equations (27) and (28).

To obtain the correlation function, we calculate the differentiation of the above CVM equations with respect to field h_1,

and then take the limit $h_i = 0$ for all i. We define the response of the Lagrangian multipliers λ_{1i}–λ_{4i} to h_1 as

$$\chi_{1i} \equiv \frac{\partial \lambda_{1i}}{\partial h_1}\Big|_{\{h_i\}=0}, \quad \chi_{2i}(z) \equiv \frac{\partial \lambda_{2i}(z)}{\partial h_1}\Big|_{\{h_i\}=0},$$
$$\chi_{3i}(z) \equiv \frac{\partial \lambda_{3i}(z)}{\partial h_1}\Big|_{\{h_i\}=0}, \quad \chi_{4i} \equiv \frac{\partial \lambda_{4i}}{\partial h_1}\Big|_{\{h_i\}=0}. \tag{39}$$

Note that since $\lambda_{2i}(z)$ and $\lambda_{3i}(z)$ contain the mean field exerted on the clusters i and $(i, i+1)$ (see discussion below Eq. (31)), $\chi_{2i}(z)$ and $\chi_{3i}(z)$ contain the response of the mean field to the external field.

Substituting Eqs. (37) and (38) into Eq. (35), doing the derivative of h_1, and taking the limit $h_i = 0$ for all i, we obtain a set of self-consistent equations about χ_{1i}, $\chi_{2i}(z)$, $\chi_{3i}(z)$, and χ_{4i}, where the CVM uniform solutions for λ_1, $\lambda_2(z)$, λ_4, and $\rho^{(1)}(z)$ are used as input. The equations can be simplified in the momentum space by introducing the Fourier transform of χ_{1i}, $\chi_{2i}(z)$, $\chi_{3i}(z)$, and χ_{4i},

$$\chi_{\alpha k} \equiv \sum_{j=1}^{L} \chi_{\alpha j} \mathrm{e}^{-\mathrm{i}k(j-1)}, \quad (\alpha = 1,2,3,4). \tag{40}$$

Here, $k = 2\pi m/L$ ($m = 0, 1, \ldots, L-1$). The self-consistent equations for $\chi_{\alpha k}$ (α = 1–4) are finally obtained as

$$\begin{aligned}
\chi_{1k} &= \int_{-\infty}^{\infty} \mathrm{d}z \rho^{(1)}(z) \left[\chi_{2k}(z) + \chi_{3k}(z) - B(z)\right], \\
\chi_{4k} &= -\iint_{-\infty}^{+\infty} \mathrm{d}z\mathrm{d}w \rho^{(2)}(z,w) \left[\chi_{2k}(z) + \mathrm{e}^{\mathrm{i}k}\chi_{3k}(w)\right], \\
\chi_{2k}(z) &= B(z) + \chi_{1k} + \mathrm{e}^{-\mathrm{i}k}\chi_{4k} \\
&\quad + \mathrm{e}^{-\mathrm{i}k}\left[\int_{-\infty}^{+\infty} \mathrm{d}w F(w,z)\chi_{2k}(w)\right], \\
\chi_{3k}(z) &= B(z) + \chi_{1k} + \chi_{4k} \\
&\quad + \mathrm{e}^{\mathrm{i}k}\left[\int_{-\infty}^{+\infty} \mathrm{d}w F(w,z)\chi_{3k}(w)\right].
\end{aligned} \tag{41}$$

In the above equations, the function $F(w,z)$ is given by

$$F(w,z) = \mathrm{e}^{\beta[-V(w,z)+\lambda_2(w)-Q(z)]}. \tag{42}$$

Here, $\lambda_2(w)$ and $Q(z)$ are solved from Eq. (31).

After Eq. (41) is solved to produce χ_{1k}, χ_{2k}, χ_{3k} and χ_{4k}, the correlation function $C_{1i} \equiv \langle B(x_1)B(x_i)\rangle - \langle B(x_1)\rangle\langle B(x_i)\rangle$ can be calculated as

$$\begin{aligned}
C_{1i} &= \frac{1}{\beta}\frac{\partial \langle B(x_i)\rangle}{\partial h_1}\Big|_{\{h_i=0\}} \\
&= \int_{-\infty}^{+\infty} \mathrm{d}z \rho^{(1)}(z) B(z) \\
&\quad \times \left[-\delta_{1,i}B(z) - \chi_{1i} + \chi_{2i}(z) + \chi_{3i}(z)\right].
\end{aligned} \tag{43}$$

The corresponding formula in momentum space reads

$$\begin{aligned}
C(k) &= \int_{-\infty}^{\infty} \mathrm{d}z \rho^{(1)}(z) B(z) \\
&\quad \times \left[-B(z) - \chi_{1k} + \chi_{2k}(z) + \chi_{3k}(z)\right],
\end{aligned} \tag{44}$$

which can give C_{1j} through

$$C_{1j} = \frac{1}{L}\sum_k C(k)\mathrm{e}^{\mathrm{i}k(j-1)}. \tag{45}$$

In Eq. (41), we can assign $\chi_{3k}(z) = \chi_{2k}^*(z)$ to obtain a real $C(k)$.

Note that Eqs. (41) and (44) depend on the system size L through the k discretization. They are exact for the thermodynamic limit $L = \infty$ but not for a chain with finite length L. The same is true for Eq. (45).

4. Results

In this section, we present the results obtained from the numerical solution of the CVM and LRT equations. We also give the asymptotic expressions valid in the low and high temperature limits. The results are for parameters $K = 1$ and $\gamma = 1$. For the numerical integration in Eqs. (31) and (41), we use the Gauss–Hermite quadrature based on 800 points of weights and meshes generated by Matlab software. We investigate the following quantities: (A) single-site reduced density $\rho^{(1)}(z)$, (B) $\langle|z|^n\rangle$, $\langle z^2\rangle$, $\langle(z_1 - z_2)^2\rangle$, (C) specific heat, and (D) static correlation function. Only (D) involves the LRT calculation.

4.1. Single-site reduced density $\rho^{(1)}(z)$

In Fig. 1, we show the single-site reduced density $\rho^{(1)}(z)$ at $z > 0$ for two representative n values, $n = 2$ (harmonic oscillator) and $n = 4$ (ϕ^4 model). Due to $\rho^{(1)}(-z) = \rho^{(1)}(z)$, the $z < 0$ regime is not shown. Other n values give similar bell-like one-peak curves with maximum at $z = 0$. With increasing temperature, the peak of $\rho^{(1)}(z)$ becomes broader and lower. Below, we will denote $\rho^{(1)}(z)$ at temperature T as $\rho^{(1)}(z,T)$. For a given n, the height of the peak, $H(n,T) \equiv \rho^{(1)}(z=0,T)$, is a decreasing function of T. The shape of the curve $\rho^{(1)}(z)$ reflects the competition between the thermal movement of particles and the shape of confining potential $|z|^n$. For a fixed T, as n increases, the local potential becomes flatter at bottom in $-1 \leqslant z \leqslant 1$ and increases more sharply at $z = \pm 1$. As a result, $\rho^{(1)}(z)$ has a flatter distribution at $|z| \leqslant 1$ and decreases sharply at $|z| \geqslant 1$. In the limit of $n = \infty$, the local potential becomes an infinitely deep potential well in $|z| \leqslant 1$ with a flat bottom. $\rho^{(1)}(z)$ will then have a rectangular-shaped distribution in $|z| \leq 1$.

In Fig. 2, we plot the peak height $H(n,T)$ as functions of T for various n values. It has different low and high temperature asymptotic power laws. Fitting the numerical data gives the following form:

$$H(n,T) \sim \begin{cases} T^{-\frac{2}{n+2}}, & (T \ll T_{\mathrm{cr}}); \\ T^{-\frac{1}{n}}, & (T \gg T_{\mathrm{cr}}). \end{cases} \tag{46}$$

For $2.0 \leqslant n \leqslant 10.0$ shown in Fig. 2, the crossover temperature $T_{\rm cr} \sim 1$, without significant n dependence. For $n = 2$, the low and high temperature exponents coincide. We have $H(n=2,T) \sim T^{-1/2}$ in the full temperature regime.

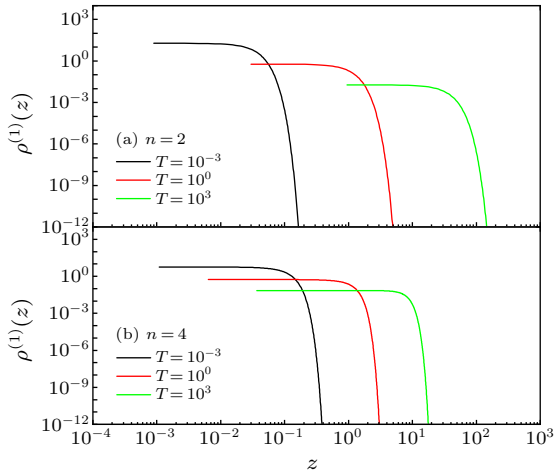


Fig. 1. Single-site reduced density $\rho^{(1)}(z)$ as a function of z for different temperatures. (a) $n = 2$ and (b) $n = 4$.

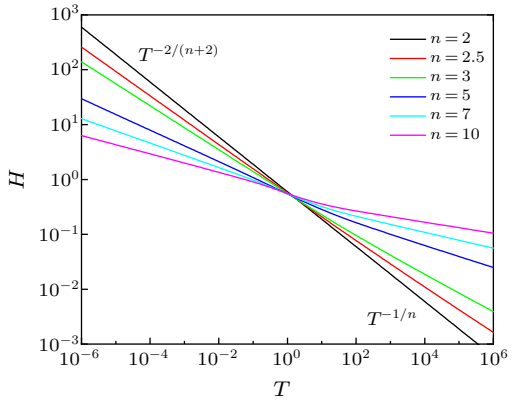


Fig. 2. The hight H of $\rho^{(1)}(z)$ curve as a function of T for various n values. The low temperature asymptotic behavior $H \sim T^{-\frac{2}{n+2}}$ and the high temperature $H \sim T^{-\frac{1}{n}}$ are marked in the figure.

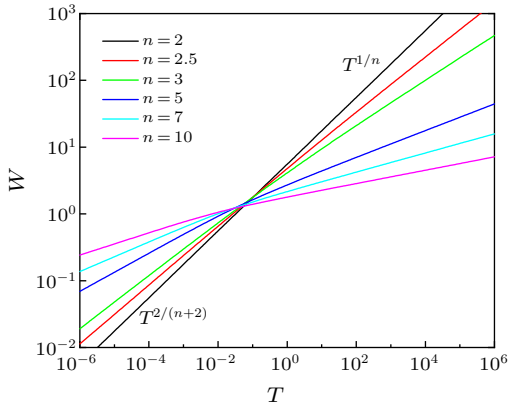


Fig. 3. Width W of $\rho^{(1)}(z)$ curve as a function of T for various n values. The low temperature asymptotic behavior $W \sim T^{\frac{2}{n+2}}$ and the high temperature $\rho^{(1)}(z) \sim T^{\frac{1}{n}}$ are marked in the figure.

In Fig. 3, we show the peak width $W(n,T)$ of the curve $\rho^{(1)}(z)$ as a function of T for different n values. $W(n,T)$ is defined as twice the positive solution z of the equation $\rho^{(1)}(z,T)/\rho^{(1)}(z=0,T) = c$ for $c = 10^{-15}$. Not surprisingly, $W(n,T)$ is inversely proportional to $H(n,T)$,

$$W(n,T) \sim \begin{cases} T^{\frac{2}{n+2}}, & (T \ll T_{\rm cr}); \\ T^{\frac{1}{n}}, & (T \gg T_{\rm cr}). \end{cases} \tag{47}$$

This is expected from the conservation of area of the $\rho^{(1)}(z)$ curve, $\int {\rm d}z \rho^{(1)}(z) = 1$. Note that the crossover temperature $T_{\rm cr} \sim 0.1$ is smaller than the value of Eq. (46), reflecting that the shape of the curve $\rho^{(1)}(z)$ evolves with n.

The two-segment behavior of $H(n,T)$ and $W(n,T)$ as functions of T shows that the oscillators' movement in the KG model is dominated by different factors in the high and low temperature limits. In the high temperature limit, due to the large amplitude of oscillations, the local potential $|z|^n$ dominates the movement and the particles are more independent. The approximate energy conservation of a local oscillator gives $W^n \sim T/2$, leading to $W \sim T^{1/n}$. In the low temperature limit, the oscillators move near the bottom of the potential well and are influenced jointly by the local potential and the non-local interaction $(z_1 - z_2)^2$ in a more subtle way, giving rise to the nontrivial behavior $W \sim T^{2/(n+2)}$.

From the two-segment power law behavior of the height $H(n,T)$ and width $W(n,T)$, one expects certain scaling behaviors in the function of $\rho^{(1)}(z,T)$ in the low and high temperature limits. In Fig. 4(a), we plot $-\ln[\rho^{(1)}(z,T)/\rho^{(1)}(0,T)]$, the minus log of $\rho^{(1)}(z,T)$ rescaled by its height at $z = 0$, as functions of z for $n = 6$ at temperatures from 10^{-6} to 10^{6}. All curves behave as z^2 for small z and z^6 for large z, separated by a temperature dependent crossover $z_{\rm cr}$. As temperature increases, the curves move towards right at different speed in the low and high temperature regimes.

In Figs. 4(b) and 4(c), we separately plot the low and high temperature data of Fig. 4(a), with z rescaled by the width of $\rho^{(1)}(z)$, i.e., by $T^{2/(n+2)}$ in the low temperature limit, and by $T^{1/n}$ in the high temperature limit, respectively (see Eq. (47)). In Fig. 4(b), all curves in the low temperatures $T = 10^{-6}$–10^{-1} nicely merge into a quadratic function in the small z regime, once z is scaled by the low temperature width power $T^{2/(n+2)}$. In the large z regime, they do not merge into a power law curve. The crossover occurs at $z/T^{\frac{2}{n+2}} \sim 1$. We have checked that the above behavior holds for all $n > 2$. The findings of Fig. 4(b) can be summarized as the following scaling form for $n > 2$,

$$\rho^{(1)}(z,T) = \rho_0 T^{-\frac{2}{n+2}} {\rm e}^{-a\left[z/T^{\frac{2}{n+2}}\right]^2}, \quad (z/T^{\frac{2}{n+2}} \ll 1,\ T \ll 1). \tag{48}$$

The coefficient $a \approx 1.0$ has a very weak dependence on n.

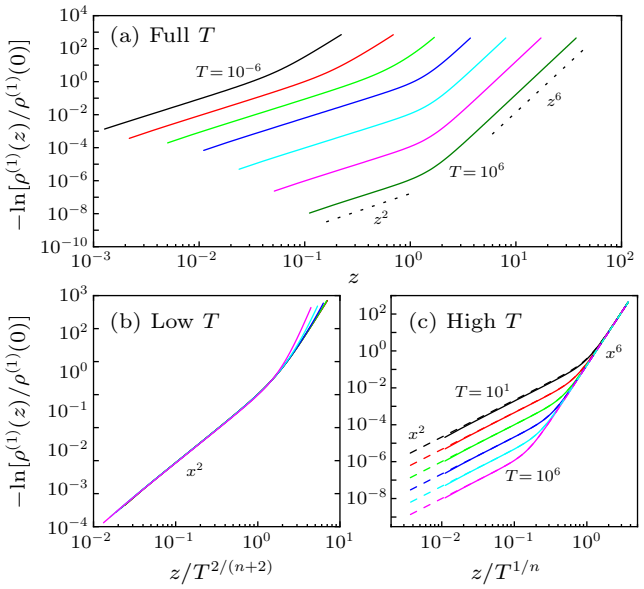


Fig. 4. Curves of $-\ln[\rho^{(1)}(z)/\rho^{(1)}(0)]$ for $n=6$ as functions of rescaled z. (a) $-\ln[\rho^{(1)}(z)/\rho^{(1)}(0)]$ as a function of z for $T=10^{-6}, 10^{-4},\ldots, 10^{6}$ (from left to right). Black dotted lines marked out the power law behavior. (b) $-\ln[\rho^{(1)}(z)/\rho^{(1)}(0)]$ as a function of $z/T^{2/(n+2)}$ for low temperatures $T=10^{-6}$–10^{-1}. (c) $-\ln[\rho^{(1)}(z)/\rho^{(1)}(0)]$ as a function of $z/T^{1/n}$ for high temperatures $T=10^{1}$–10^{6} (from left to right). The dashed lines are curves for $-\beta(|z|^n/n+z^2)$ vs. $z/T^{1/n}$. The power functions x^2 and x^6 are marked in the figures.

In the high temperature limit, we scale z by the high temperature width power $T^{1/n}$ and re-plot the high temperature curves of Fig. 4(a) in Fig. 4(c). We find that $\rho^{(1)}(z,T)$ has a scaling form only in the large z regime. Considering that the non-local coupling plays no role in this limit, one can estimate $\rho^{(1)}(z_i)$ by $\iint \mathrm{e}^{-\beta\left[|z_i|^n/n+(z_i-z_{i-1})^2/2+(z_{i+1}-z_i)^2/2\right]}\mathrm{d}z_{i-1}\mathrm{d}z_{i+1}$, giving $\rho^{(1)}(z_i)\sim \mathrm{e}^{-\beta(|z_i|^n/n+z_i^2)}$. This formula (dashed lines) nicely matches the whole curves in Fig. 4(c). We thus obtain the high temperature asymptotic behavior of $\rho^{(1)}(z,T)$ (for $n>2$) as

$$\rho^{(1)}(z,T)=\rho_0 T^{-\frac{1}{n}}\,\mathrm{e}^{-\frac{1}{T}\left(\frac{|z|^n}{n}+z^2\right)},\quad (T\gg 1). \tag{49}$$

A more systematic derivation of Eq. (49) from CVM equations is given in Appendix A. In the large z limit, the $|z|^n$ term dominates the exponent (for $n>2$) and the above equation becomes a scaling form $\rho^{(1)}(z,T)\sim T^{-\frac{1}{n}}\rho^{(1)}(z/T^{\frac{1}{n}},1)$. This then gives a well-defined width $W(n,T)\sim T^{\frac{1}{n}}$, being consistent with Eq. (47).

For $n=2$, the local and non-local potentials have the same power. The above analysis for high temperature does not hold anymore because the non-local interaction cannot be ignored even in the high temperature limit. However, the form of Eq. (48) covers Eq. (49) in this case. So we have for $n=2$,

$$\rho^{(1)}(z,T)(n=2)=\rho_0 T^{-\frac{1}{2}}\,\mathrm{e}^{-az^2/T}. \tag{50}$$

Fitting the numerical data of $\rho^{(1)}(z,T)$ $(n=2)$ with this equation gives $a\approx 1.1$.

4.2. $\langle|z|^m\rangle$ and $\langle(z_1-z_2)^2\rangle$

In this part, we study the thermodynamic averages $\langle|z|^m\rangle$ for arbitrary m and the average of nearest-neighbor coupling $\langle(z_1-z_2)^2\rangle$. $\langle|z|^m\rangle$ can be calculated directly from the single-site reduced density $\rho^{(1)}(z,T)$ through

$$\langle|z|^m\rangle=\int_{-\infty}^{+\infty}|z|^m\rho^{(1)}(z,T)\mathrm{d}z. \tag{51}$$

Using the low and high temperature expressions for $\rho^{(1)}(z,T)$ Eqs. (48) and (49), we obtain the low and high temperature asymptotic behavior of $\langle|z|^m\rangle$ as

$$\langle|z|^m\rangle\sim\begin{cases} T^{\frac{2m}{n+2}}, & (T\ll T_{\mathrm{cr}});\\ T^{\frac{m}{n}}, & (T\gg T_{\mathrm{cr}}).\end{cases} \tag{52}$$

Note that in the high temperature limit, the width of $\rho^{(1)}(z,T)$ becomes so large that the integration in Eq. (51) will be dominated by the $|z|^n$ term in the expression of $\rho^{(1)}(z,T)$, Eq. (49). So the high temperature behavior $\langle|z|^m\rangle\sim T^{m/n}$ is the properties of the atomic limit, as analyzed in Appendix A.

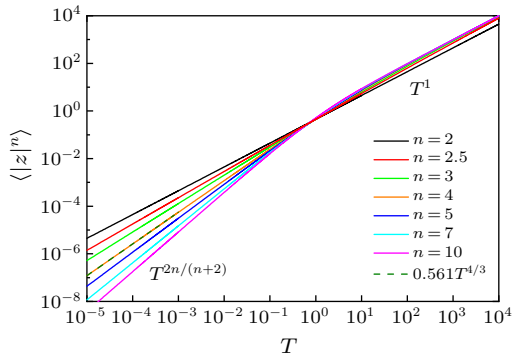


Fig. 5. The $\langle|z|^n\rangle$ as a function of temperature T for various n values. The low and high temperature asymptotic power laws are marked in the figure. The dashed line is for $0.561T^{4/3}$ obtained in Ref. [22] for ϕ^4 lattice model (KG model at $n=4$) in the low temperature limit.

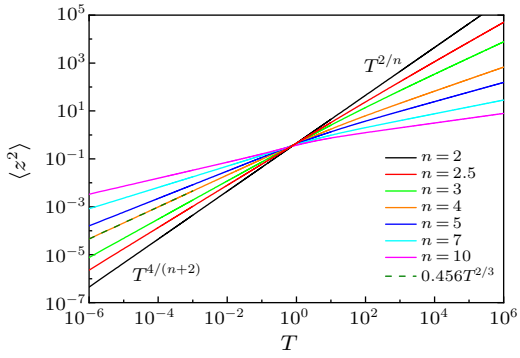


Fig. 6. The $\langle z^2\rangle$ as a function of temperature T for various n values. The low and high temperature asymptotic power laws are marked in the figure. The dashed line is for $0.456T^{2/3}$ obtained in Ref. [22] for ϕ^4 lattice model $(n=4)$ in the low temperature limit.

In Figs. 5 and 6, we plot the numerical results for $\langle|z|^n\rangle(T)$ and $\langle z^2\rangle(T)$, respectively, for various n values. These curves fulfil the asymptotic low and high temperature power

laws in Eq. (52), with a crossover at around $T_{\rm cr} \sim 1$. For $n = 2$, the low and high temperature limits have the same asymptotic power $T^{m/2}$ for arbitrary m. We did not observe any signature of crossover between the low and high temperature regimes (see the $n = 2$ curves in Figs. 5 and 6). This supports that for $n = 2$, there is a unified power law function in the full temperature regime, i.e., Eq. (50). For $n = 4$, the exact low temperature asymptotic expression has been obtained as $\langle z^2\rangle = 0.456T^{2/3}$ and $\langle z^4\rangle = 0.456T^{4/3}$ from the analysis of the corresponding quantum anharmonic oscillator in the high temperature limit.[22] As shown by the dashed lines in Figs. 5 and 6, CVM data agree well with these formulas in the low temperature limit. The same expressions agree well with the MD simulation data in the low temperature regime,[20] constituting a cross validation of all methods.

Here, it is appropriate to discuss the self-consistency between CVM and LRT. As noted at the end of Subsections 3.1 and 3.2, the system size L does not appear in our CVM formula for the periodic boundary condition. It appears in the LRT formula only through the summation of k in Eq. (45). The LRT result from Eq. (45) should be consistent with the CVM result from $\rho^{(1)}(z)$ (Eq. (29)) and $\rho^{(2)}(z,w)$ (Eq. (30)) in the limit $L = \infty$ where both are expected to be exact. This consistency is a test of exactness of the theory. We consider the local quantity $\langle z^2\rangle$ which can be calculated from CVM and LRT respectively through

$$\langle z^2\rangle_{\rm CVM} = \int_{-\infty}^{+\infty} z^2\rho^{(1)}(z,T)\,{\rm d}z,$$
$$\langle z^2\rangle_{\rm LRT} = C_{11} = \frac{1}{L}\sum_k C(k). \tag{53}$$

Here, C_{11} and $C(k)$ are given in Eqs. (43) and (45), respectively. It turns out that for finite L, LRT always produces larger $\langle z^2\rangle$ than CVM. We gauge the finite size error in $\langle z^2\rangle_{\rm LRT}$ by $\delta\langle z^2\rangle \equiv \langle z^2\rangle_{\rm LRT} - \langle z^2\rangle_{\rm CVM}$. In Fig. 7, we plot $\delta\langle z^2\rangle$ as functions of L for a series of temperatures at $n = 4$. They decay exponentially with increasing L, tending to zero in the thermodynamic limit. This confirms the expected consistency between CVM and LRT. We define the decay length $\xi_{\rm size}$ as $\delta\langle z^2\rangle = c\,{\rm e}^{-L/\xi_{\rm size}}$. The inset of Fig. 7 shows that $\xi_{\rm size}(T)$ decreases with increasing T and coincides with the correlation length $\xi_{\rm corr}(T)$ extracted from the correlation function $C_{1i} \propto {\rm e}^{-(i-1)/\xi_{\rm corr}}$ in the large i limit. This is a reasonable result since the finite size error can be measured by how much long-range correlation beyond the system size is neglected in the finite size calculation. It is therefore controlled by $L/\xi_{\rm corr}$.

It should be noted that $\langle z^2\rangle_{\rm LRT}$ is not the exact result for a chain with finite length L. This is because CVM is exact for system with an open boundary condition, while in the derivation of LRT, we have used the Fourier transformation which applies only to periodic systems. Thus the combination of CVM and LRT is exact only in the thermodynamic limit. In fact, we have checked that for small L, $\langle z^2\rangle_{\rm LRT}(T)$ has an incorrect power law in the temperature dependence in the low temperature limit.

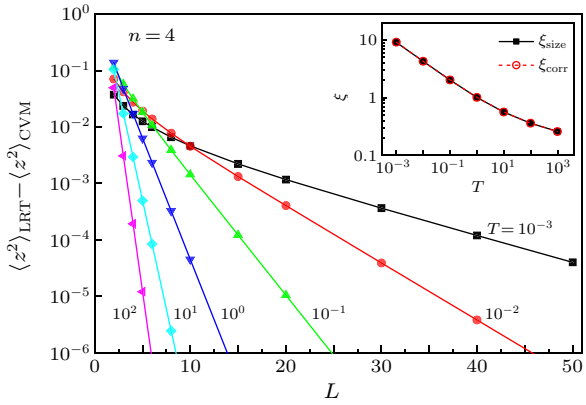


Fig. 7. The difference between $\langle z^2\rangle$'s obtained from LRT (Eq. (45)) and CVM (Eq. (51)) as a function of L for $n = 4$ and various temperatures (marked in the figure). Inset: decay length $\xi_{\rm size}(T)$ from fitting the exponential decay in the main figure (squares with solid guiding line), and the correlation length $\xi_{\rm corr}(T)$ from fitting the correlation function via Eq. (60) (cycles with dashed guiding lines).

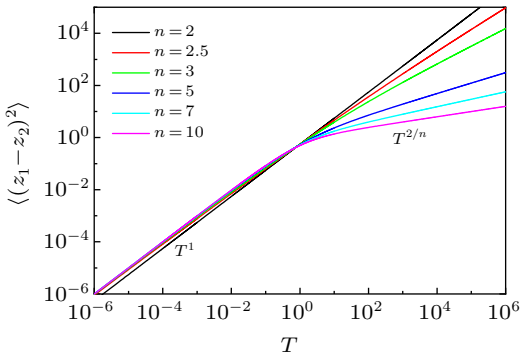


Fig. 8. The $\langle (z_1 - z_2)^2\rangle$ as a function of temperature T for various n values. The low and high temperature asymptotic power laws are marked.

The average $\langle (z_1 - z_2)^2\rangle$ involves the correlation between the displacements z_1 and z_2 of the two nearest sites. It must be calculated from $\rho^{(2)}(z,w)$ of Eq. (30). In Fig. 8, $\langle (z_1 - z_2)^2\rangle(T)$ as functions of T is plotted for various n values. Similar two-segment behavior is observed, with the asymptotic behavior extracted as

$$\langle (z_1 - z_2)^2\rangle \sim \begin{cases} T^1, & (T \ll T_{\rm cr}); \\ T^{\frac{2}{n}}, & (T \gg T_{\rm cr}), \end{cases} \tag{54}$$

with $T_{\rm cr} \sim 1.0$. In the high temperature limit, the correlations between neighboring sites can be neglected, we have $\langle (z_1 - z_2)^2\rangle \sim 2\langle z^2\rangle \sim T^{2/n}$. In the low temperature limit, $\langle (z_1 - z_2)^2\rangle = 2(\langle z^2\rangle - \langle z_1 z_2\rangle)$. Since for $n > 2$ and $T \to 0$, $\langle z^2\rangle \sim T^{4/(n+2)}$ is much larger than $\langle (z_1 - z_2)^2\rangle \sim T^1$, we expect that the T^1 behavior in the latter is the result of a cancelation of the leading $T^{4/(n+2)}$ term in both $\langle z^2\rangle$ and $\langle z_1 z_2\rangle$. This shows that in the low temperature limit, the nearest-neighbor correlation of x_i is as large as the local correlation. We see that

the temperature behavior of the averages is characterized by a two-segment fashion, with the high T properties dominated by the local potential, and the low T properties determined jointly by the local potential and the non-local interaction.

4.3. Specific heat

The internal energy $\langle H\rangle$ for the KG lattice model is expressed in terms of the averages discussed in the previous subsection

$$\langle H\rangle = \frac{1}{2}TL + \frac{L}{2}\langle (z_1 - z_2)^2\rangle + \frac{L}{n}\langle |z|^n\rangle. \tag{55}$$

The specific heat can be obtained from $C_{\rm v} = (1/L)\partial\langle H\rangle/\partial T$.

In Fig. 9, we plot $C_{\rm v}$ as functions of T for various n values. For $n > 2$, $C_{\rm v}(T)$ is a decreasing function of T. We observe $C_{\rm v} = 1.0$ at $T = 0$ and it decreases to a constant smaller than unity in the high temperature limit. The crossover temperature separating the low and the high temperature plateaus is about $T_{\rm cr} = 10^{-2}$–10^{0} for $2 < n < 10$. For the special case $n = 2$, $C_{\rm v} = 1$ for all temperatures, as expected from the energy equipartition theorem. The inset shows that $C_{\rm v}(T = \infty)$ agrees well with $1/2 + 1/n$. For $n = 4$, the curve $C_{\rm v}(T)$ and the high temperature value $3/4$ agree with the results from projective truncation approximation for ϕ^4 lattice model.[18] The obtained low and high temperature asymptotic values of $C_{\rm v}$ for $n \geqslant 2$ are thus summarized as

$$C_{\rm v} = \begin{cases} 1, & (T \ll 1); \\ \frac{1}{2} + \frac{1}{n}, & (T \gg 1). \end{cases} \tag{56}$$

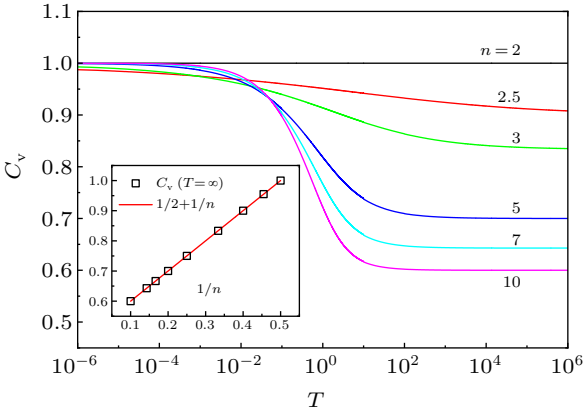


Fig. 9. Specific heat $C_{\rm v}$ as a function of temperature T for various n values. The inset shows the extrapolated value of $C_{\rm v}(\infty)$ (squares) versus $1/n$ (solid line), showing $C_{\rm v}(\infty) = 1/2 + 1/n$.

This result can be understood in terms of previous results. According to Eqs. (52) and (54), we write the asymptotic expression for $\langle (z_1 - z_2)^2\rangle$ and $\langle |z|^n\rangle$ as

$$\langle (z_1 - z_2)^2\rangle \sim \begin{cases} AT^1, & (T \ll 1); \\ \tilde{A}T^{\frac{2}{n}}, & (T \gg 1); \end{cases} \tag{57}$$

$$\langle |z|^n\rangle \sim \begin{cases} BT^{\frac{2n}{n+2}}, & (T \ll 1); \\ \tilde{B}T^1, & (T \gg 1). \end{cases} \tag{58}$$

Here, A, $\tilde{A}$, B, and $\tilde{B}$ are temperature-independent coefficients in the asymptotic limits. Inserting the above two equations into Eq. (55), we obtain for $n > 2$

$$C_{\rm v} = \begin{cases} \frac{1}{2} + \frac{1}{2}A + \frac{2}{n+2}BT^{\frac{n-2}{n+2}}, & (T \ll 1), \\ \frac{1}{2} + \frac{1}{n}\tilde{B} + \frac{1}{n}\tilde{A}T^{\frac{2}{n}-1}, & (T \gg 1). \end{cases} \tag{59}$$

For $T \ll 1.0$, the system becomes quadratic and equipartition of energy gives $A = 1.0$. For $T \gg 1.0$, from the high temperature asymptotic expression of $\rho^{(1)}(z,T)$ in Eq. (49), one can rigorously derive $\tilde{B} = 1$. Inserting these into Eq. (59), one obtains the observed result Eq. (56) for $n > 2$. For $n = 2$, we expect that $A(n=2) + B(n=2) = 1$ and $\tilde{A}(n=2) + \tilde{B}(n=2) = 1$, as required by $C_{\rm v}(n=2) = 1.0$. The crossover temperature of $C_{\rm v}(T)$ can be estimated by equating the low and high temperature expressions in Eq. (59).

As a qualitative understanding of Eq. (56), we note that for the classical system with continuous variables, the temperature is a measure of the total energy density $\langle H\rangle/L$. Hence $\langle H\rangle/L \sim T$ always holds for arbitrary potential and interaction, giving out basically constant specific heat $C_{\rm v}$. However, the value of T-linear coefficient of $\langle H\rangle/L$ depends on details of the potential and interaction. Here for the KG lattice model Eq. (1), the local potential $\frac{1}{n}|x|^n$ controls the high temperature behavior. With increasing n, the potential energy decreases rapidly (due to both the $1/n$ factor and the form $|x_i|^n$) in the accessible spatial area of atoms and thus makes less contribution $\frac{1}{n}$ to the high temperature specific heat $C_{\rm v} = \frac{1}{2} + \frac{1}{n}$.

4.4. Static correlation function

The static correlation function $C_{1i} = \langle x_1 x_i\rangle - \langle x_1\rangle\langle x_i\rangle$ is calculated from LRT formula Eqs. (44) and (45) for a sufficiently long chain, choosing the function $B(x) \equiv x$. For the present model, $\langle x_i\rangle = 0$. Figure 10 shows that C_{1i} decays exponentially with increasing i for any temperature, starting from $i = 1$ and until i is close to $L/2$. We therefore define the correlation length ξ as

$$C_{1i} = \langle x^2\rangle \, {\rm e}^{-\frac{i-1}{\xi}}, \quad (1 \leq i \ll L/2). \tag{60}$$

Figure 10(a) shows that for $n = 2$, ξ is a constant independent of T. Figure 10(b) shows that for $n = 4$, ξ is a decreasing function of temperature.

The temperature dependence of correlation length ξ is presented in Fig. 11 for various n values. For $n = 2$, our fitting gives the T-independent value $\xi(T) = 1.03904$, in good agreement with the exact value $1/\ln[(3+\sqrt{5})/2]$ (see the PTA result in Subsection 4.5). For $n > 2$, $\xi(T)$ diverges in a power law fashion $\xi \sim T^{\theta<0}$ in the low temperature limit. In the large T limit, $\xi(T)$ decreases slower than the power law. It is interesting to notice that the curves of $\xi(T)$ for different n values cross a common point at $T = T_{\rm c} \approx 1.0$ and $\xi_{\rm c} \approx 1.0$.

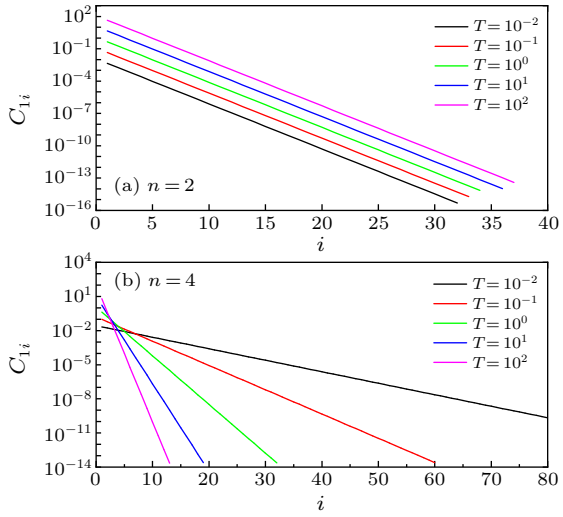


Fig. 10. Correlation function C_{1i} as a function of lattice site index i, for (a) $n=2$ and (b) $n=4$ at various temperatures.

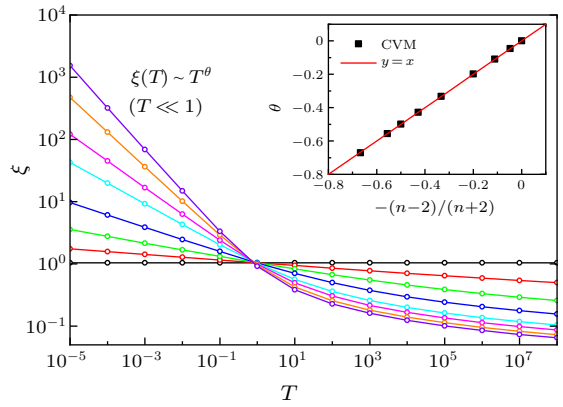


Fig. 11. Correlation length ξ as functions of temperature T for various n values. From bottom to top on the left side, $n=2.0$, 2.2, 2.5, 3.0, 4.0, 5.0, 7.0, and 10.0. The symbols are data and lines are for guiding the eyes. Inset: low temperature asymptotic power θ from $\xi(T\ll T_{\rm cr})\sim T^{\theta}$ versus $-(n-2)/(n+2)$ (solid squares), compared with the function $y=x$ (red line).

Numerical fitting reveals the following asymptotic power law behavior of $\xi(T)$ in the low temperature limit:

$$\xi(T)\sim T^{-\frac{n-2}{n+2}},\quad (T\ll T_{\rm cr}). \tag{61}$$

See inset of Fig. 11. In the high temperature regime, combining the numerical fitting with the asymptotic analysis in Appendix A, we extract the asymptotic behavior of $\xi(T\gg T_{\rm cr})$ (see Fig. 12) as

$$\xi(T)=\frac{1}{a_n\ln T+b_n},\quad (n>2,\ T\gg T_{\rm cr}), \tag{62}$$

with

$$a_n=\frac{n-2}{n},\quad b_n=\ln\left[n^{-\frac{2}{n}}\frac{\Gamma(\frac{1}{n})}{\Gamma(\frac{3}{n})}\right]. \tag{63}$$

In Figs. 12(a) and 12(b), we show the high temperature data for $1/\xi(T)$ for various n values, showing that they are linear function of $\ln T$ for sufficiently large T. The smaller n is, the larger T is needed to observe the linearity, as seen by comparing data in Figs. 12(a) and 12(b). In Fig. 12(c), the numerical fitted coefficients a_n and b_n agree well with Eq. (63) except for n very close to 2. This is because for $n\to 2+$, one needs to go to extremely high T to observe the behavior of Eq. (62). In Appendix A, we give the details of the derivation of Eqs. (62) and (63).

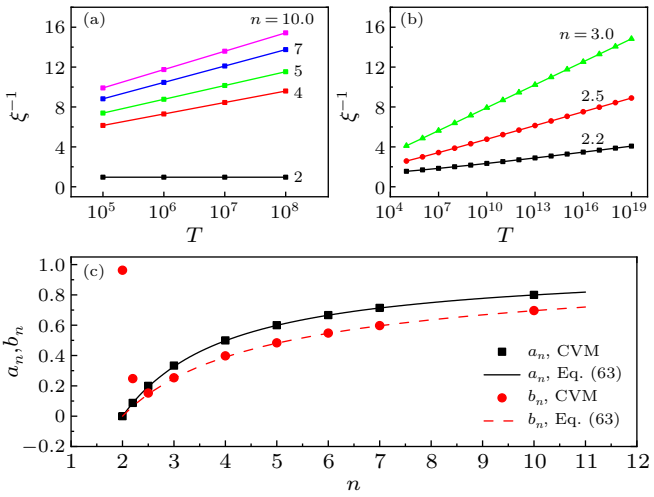


Fig. 12. (a) and (b) Inverse correlation length ξ^{-1} as a function of T in the high temperature regime for various n values. The n values are marked in the figure. In panel (c), the fitted power a_n and b_n from CVM data according to $\xi^{-1}(T\gg T_{\rm cr})=a_n\ln T+b_n$ (squares and dots) are compared to Eq. (63) (solid and dashed lines).

The crossover temperature $T_{\rm cr}$ in $\xi(T)$ can be estimated by equating Eqs. (61) and (62). We obtain $T_{\rm cr}=c^{n/(n-2)}$ with $c>1$ being a constant. As n decreases towards $n=2^{+}$, $T_{\rm cr}$ diverges and the low temperature formula Eq. (61) governs the whole temperature range. This is why for smaller n, one needs to go to larger T to observe the high temperature asymptotic behavior Eq. (63). For $n=2$, $T_{\rm cr}=\infty$. Equation (61) gives T-independent ξ, being consistent with the $n=2$ curve in Fig. 11.

4.5. Comparison with PTA

In this section, we present and analyze the PTA results for the one-dimensional KG lattice model. As was discussed in detail in Ref. [18] for the one-dimensional ϕ^4 lattice model (corresponding to KG model with $n=4$), PTA can be used to systematically study classical many-body problems. The PTA based on the simplest operator basis $B_1=\{Q_k=1/\sqrt{L}\sum_{j=1}^{L}x_j\,{\rm e}^{-{\rm i}jk}\}$ (denoted as PTA-B_1 below) is shown to be equivalent to the quadratic variational method. This method has only been tested at certain points of the parameters. Here, using the exact CVM results for the KG model as a reference, we analyze the accuracy of PTA in the full temperature range. Demonstrating with the $n=4$ case, we show that PTA-B_1 already gives qualitatively correct low and high temperature asymptotic behaviors. The PTA-B_2 based on basis $B_2=\{Q_k,R_k\}$, with $R_k=1/\sqrt{L}\sum_{j=1}^{L}x_j^3\,{\rm e}^{-{\rm i}jk}$, further im-

proves the quantitative accuracy. The analysis of the PTA-B_1 equations also provides a derivation of the low temperature asymptotic exponents of the averages $\langle x_i^m\rangle(T)$ ($m>0$ and m is even) and the correlation length $\xi(T)$, as presented in Appendix B.

To carry out PTA, one first selects a set of operators (dynamical variables for the case of classical models) as the basis. The equations of motion of Green's functions defined on these operators are then truncated by using the projection method. Here, we sketch the main formula for the one-dimensional KG model $H(K,\gamma)$ defined in Eq. (1) for even n. The final asymptotic expression also applies to the odd n case. The general formalism of PTA for classical models can be found in Ref. [18].

The B_1 basis $\{Q_k\}$ is defined as

$$Q_k = \frac{1}{\sqrt{L}}\sum_{j=1}^{L} x_j \mathrm{e}^{-\mathrm{i}jk}. \tag{64}$$

Here $k=(2\pi/L)m_k$ ($m_k=0,1,\ldots,L-1$) is the lattice momentum. We used the inner product[18] $(X|Y)\equiv\langle\{X^*,\{Y,H\}\}\rangle$. Here $\{A,B\}$ is the Poisson bracket between variables A and B. We obtain the inner product matrix $\boldsymbol{I}$ and Liouville matrix $\boldsymbol{L}$ as

$$\begin{aligned} I_{k,k'} &\equiv (Q_k|Q_{k'}) = \frac{1}{m}\delta_{kk'}, \\ L_{k,k'} &\equiv -(Q_k|\{\{Q_{k'},H\},H\}) \\ &= \frac{1}{m^2}\left[\omega_0^2(k)+(n-1)\gamma\langle x^{n-2}\rangle\right]\delta_{kk'}. \end{aligned} \tag{65}$$

The Green's function $G(Q_k|Q_k^*)_\omega$ is then obtained approximately as

$$G(Q_k|Q_k^*)_\omega \approx \frac{1/m}{\omega^2-\frac{1}{m}\left[\omega_0^2(k)+(n-1)\gamma\langle x^{n-2}\rangle\right]}. \tag{66}$$

Here, $\omega_0^2(k)=2K[1-\cos(k)]$. The averages $\langle Q_k^*Q_k\rangle$ can be calculated from the spectral theorem. It reads

$$\langle Q_k^*Q_k\rangle \approx \frac{1/\beta}{\omega_0^2(k)+(n-1)\gamma\langle x^{n-2}\rangle}. \tag{67}$$

This gives the correlation function

$$\langle x_l x_j\rangle \approx \frac{1}{\beta L}\sum_k \frac{\mathrm{e}^{\mathrm{i}k(j-l)}}{\omega_0^2(k)+(n-1)\gamma\langle x^{n-2}\rangle} \tag{68}$$

and the average $\langle x^2\rangle$

$$\langle x^2\rangle \approx \frac{1}{\beta L}\sum_k \frac{1}{\omega_0^2(k)+(n-1)\gamma\langle x^{n-2}\rangle}. \tag{69}$$

To solve the unknown $\langle x^{n-2}\rangle$ appearing in the above equations self-consistently, we need to extend the EOM to the Green's functions $G(Q_k|R^*(m)_k)_\omega$, with $R(m)_k\equiv 1/\sqrt{L}\sum_j (x_j)^m \mathrm{e}^{-\mathrm{i}jk}$. We have $Q_k=R(1)_k$. The EOM and PTA for these extended GFs, together with the spectral theorem, lead to the following recursive relation for arbitrary odd $m>0$:

$$\langle x^{m+1}\rangle \approx m\langle x^2\rangle\langle x^{m-1}\rangle. \tag{70}$$

Using this equation, we can simplify Eq. (69) into

$$\langle x^2\rangle \approx \frac{1}{\beta L}\sum_k \frac{1}{\omega_0^2(k)+(n-1)!!\gamma\langle x^2\rangle^{n/2-1}}. \tag{71}$$

From the above equations for $\langle x^2\rangle$ and $\langle Q_k^*Q_k\rangle$, we can analyze the low and high temperature asymptotic behavior of the averages $\langle x^m\rangle(T)$ and $\xi(T)$ from PTA-B_1. We put the details of analysis into Appendix B and only present the results here. For $n>2$, the asymptotic behavior of $\langle x^m\rangle$ (for even m) reads

$$\langle x^m\rangle_{\mathrm{PTA}}(T) \approx \begin{cases} c_1 T^{\frac{2m}{n+2}}, & (T\ll 1); \\ c_2 T^{\frac{m}{n}}, & (T\gg 1). \end{cases} \tag{72}$$

Here, $c_1=(m-1)!!\left[16K\gamma(n-1)!!\right]^{-m/(n+2)}$, and $c_2=(m-1)!!\left[(n-1)!!\gamma\right]^{-m/n}$. Comparing them with the CVM expression Eq. (52), we find that PTA gives the correct asymptotic exponents.

The correlation length ξ is independent of T at $n=2$. It can be obtained exactly by comparing Eq. (67), which gives exact correlation function $C(k)$ for $n=2$, and the fitting expression $C^{\mathrm{fit}}(k)$ in Eq. (A16) in Appendix A. We obtain $\xi(n=2)=1/\ln[(2+r+\sqrt{r^2+4r})/2]$, with $r=\gamma/K$. For $K=\gamma=1$, it agrees well with the CVM numerical data 1.03904 in Fig. 11.

For $n\geq 2$, the asymptotic expression for the correlation length from PTA-B_1 reads

$$\xi_{\mathrm{PTA}}(T) \approx \begin{cases} d_1 T^{-\frac{n-2}{n+2}}, & (T\ll 1); \\ 1/(a_n \ln T + b_n), & (T\gg 1). \end{cases} \tag{73}$$

Here, $d_1=4K\left[16(n-1)!!K\gamma\right]^{-2/(n+2)}$, $a_n=1-2/n$, and $b_n=(2/n)\ln[(n-1)!!\gamma]-\ln K$. Compared to CVM result Eqs. (61)–(63), the PTA expression has correct form and correct a_n. But the coefficients d_1 and b_n are inaccurate. For other quantities such as $\langle(z_1-z_2)^2\rangle$ and correlation length $\xi(T)$, PTA also gives qualitatively correct asymptotic behavior.

Given the qualitative correctness of PTA results, below we make a quantitative comparison between PTA and CVM. To be specific, we use the case of $n=4$ with $K=1$ and $\gamma=1$, i.e., the ϕ^4 model that has been studied by PTA on two successively larger bases, $B_1=\{Q_k\}$ and $B_2=\{Q_k,R_k\}$.[18] We compare quantities $\langle z^4\rangle$, $\langle(z_1-z_2)^2\rangle$ (Fig. 13), and the correlation length $\xi(T)$ (Fig. 14).

In Figs. 13(a) and 13(b), we respectively plot the relative errors in the averages $\langle z^4\rangle_{\mathrm{PTA}}$ and $\langle(z_1-z_2)^2\rangle_{\mathrm{PTA}}$ with respect to CVM results as functions of temperature. It is seen that in the temperature regime from 10^{-6} to 10^6, PTA-B_2 result always has smaller error than that of PTA-B_1. The relative error

in $\langle z^4\rangle_{\rm PTA}$ on B_1 basis is smaller than 5% at all temperatures and tends to zero in the large T limit. The relative errors in $\langle(z_1-z_2)^2\rangle_{\rm PTA}$ on B_1 and B_2 bases are negative. Their absolute values are smaller than 15% at all temperatures and tend to zero in the limit $T=0$. The insets of Figs. 13(a) and 13(b) show that the curves $\langle z^4\rangle$ and $\langle(z_1-z_2)^2\rangle$ from CVM, PTA-B_1, and PTA-B_2 are indistinguishable to the eyes on the scale of the plot.

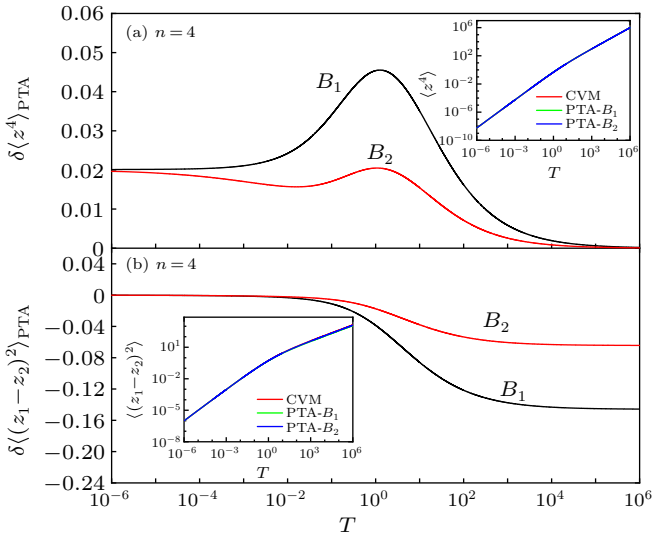


Fig. 13. Relative errors of PTA-B_1 and PTA-B_2 results with respect to CVM result for $n=4$. In (a), $\delta\langle z^4\rangle_{\rm PTA}=\left(\langle z^4\rangle_{\rm PTA}-\langle z^4\rangle_{\rm CVM}\right)/\langle z^4\rangle_{\rm CVM}$ is plotted as a function of T. In panel (b), $\delta\langle(z_1-z_2)^2\rangle_{\rm PTA}=\left[\langle(z_1-z_2)^2\rangle_{\rm PTA}-\langle(z_1-z_2)^2\rangle_{\rm CVM}\right]/\langle(z_1-z_2)^2\rangle_{\rm CVM}$ is plotted as a function of T. In both (a) and (b), the black and read curves are from B_1 and B_2 bases, respectively. In the insets of (a) and (b), $\langle z^4\rangle$ and $\langle(z_1-z_2)^2\rangle$ from different methods are shown as functions of T, respectively.

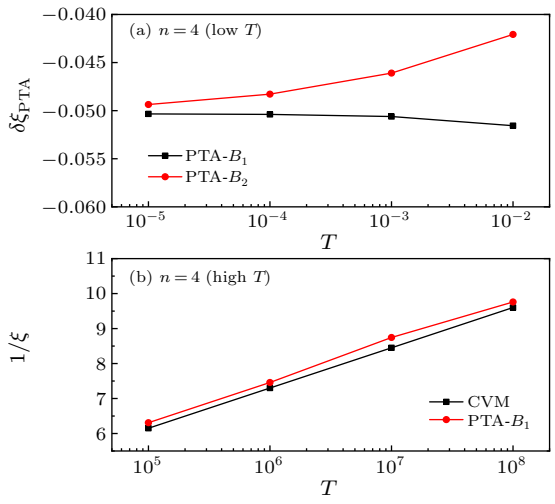


Fig. 14. (a) Relative errors $\delta\xi_{\rm PTA}$ of the correlation length, obtained from PTA-B_1 and PTA-B_2, with respect to CVM result at low temperature. Here, $\delta\xi_{\rm PTA}=(\xi_{\rm PTA}-\xi_{\rm CVM})/\xi_{\rm CVM}$. (b) Comparison of $1/\xi$ from PTA-B_1 and that from CVM at high temperature. Both (a) and (b) are for $n=4$.

Lastly, we compare the correlation length of the ϕ^4 model obtained by PTA-B_1, PTA-B_2, and CVM. Figure 14(a) shows the relative error of correlation length $\delta\xi_{\rm PTA}=(\xi_{\rm PTA}-\xi_{\rm CVM})/\xi_{\rm CVM}$ for PTA-B_1 and PTA-B_2 in the low temperature regime. Both are negative and their absolute values are on the level of 5% for $T\le 10^{-2}$. Again the relative error of PTA-B_2 has smaller absolute value than that of PTA-B_1 at all temperatures. This and similar observation in Fig. 13 show that the precision of PTA improves with increasing basis dimension. In Fig. 14(b), the high temperature part of $1/\xi(T)$ obtained from PTA-B_1 is compared with that from CVM. Both are linear curves on the linear-log plot, being consistent with Eq. (62). This confirms the qualitative correctness of PTA-B_1 in the high temperature limit. The largest relative error of PTA-B_1 in this quantity is on the order of 20%.

Overall, making use of the exact CVM results, we gauge the accuracy of PTA-B_1 and PTA-B_2 results. The comparison shows that both PTA-B_1 and PTA-B_2 give correct low and high temperature asymptotic power laws. The quantitative accuracy is improved systematically by going from B_1 basis to B_2.

5. Summary and discussion

In this paper, we implemented the CVM and LRT calculation for the one-dimensional generalized nonlinear KG lattice model, which has continuous degrees of freedom. We presented results for the single-site reduced density $\rho^{(1)}(z)$, on-site averages $\langle|z^n|\rangle$ and $\langle z^2\rangle$, nearest-neighbor coupling $\langle(z_1-z_2)^2\rangle$, specific heat $C_{\rm v}$, and correlation length ξ. We obtained their low and high temperature asymptotic scaling behaviors from both numerical and analytical analyses. Exact expressions for the asymptotic power law exponents are obtained. Using the ϕ^4 model (KG model at $n=4$), we compared the PTA results with CVM and established that PTA on the B_1 and B_2 bases gave qualitatively correct and quantitatively well-controlled results.

The CVM used in this work, i.e., CVM on the cluster of nearest-neighbor pairs and LRT, is exact for any one-dimensional lattice model with nearest-neighbor coupling and open boundary condition. Therefore, similar study can be carried out for a large class of models of this type, including Frenkel–Kontorova model,[66] ding-a-ling model,[67] and models with more complicated local potentials such as the double-well potential,[68] etc. For systems with longer-range interactions, exact thermodynamic properties can also be obtained from CVM on larger clusters if the size of the cluster can cover the interaction range.

However, it is noted that the present CVM has difficulty in studying the one-dimensional lattice models that conserve the total momentum, such as the FPU-β model,[10] Toda model,[69,70] Lennard–Jones chain model,[71] etc. This is because for these models, the continuous x_i-translation symmetry of the system makes the x_i's unconfined and hence the single-site reduced density $\rho^{(1)}(z)$ exactly zero. The formalism of CVM, which is based on $\rho^{(1)}(z)$, must be modified before it can be applied to such lattice models. This issue will be studied in the future.

It is natural to ask whether the exactness of CVM can be extended to the time domain of the classical dynamical systems to study the interested relaxation or response properties. An extension of CVM to the time domain is the path probability method.[72] It studies the kinetic process of the Ising-like lattice models and can be used to describe non-equilibrium time evolution process in alloy systems. However, a similar theory for describing the Hamilton dynamics of atoms has not been developed yet. Further study in this direction will be interesting.

Appendix A: High temperature analysis of CVM and LRT solution for $n > 2$

The CVM equations Eq. (31) can be simplified into an integral equation for $Q(z)$ as

$$\mathrm{e}^{\beta Q(z)} = \int_{-\infty}^{+\infty} \mathrm{d}w\, \mathrm{e}^{\beta[-V(z-w)-U(w)+Q(w)+\lambda_1+\lambda_4]}. \tag{A1}$$

For $n > 2$, the local term $U(w) \sim |w|^n$ exceeds the non-local term $V(z-w) \sim (z-w)^2$ in the large w regime. As a result, at high temperatures, the inter-site coupling $V(z-w)$ plays a minor role and we can expand the equations into perturbation series of $\beta V(z-w)$. In the zero-th order of $\beta V(z-w)$, one gets $Q_0(z) = Q_0$, being a constant. To get the first-order correction, one put $Q_0(z) = Q_0$ into the right-hand side of the above equation. Expanding the right-hand side of Eq. (A1) to first-order of $\beta V(z-w)$ and we obtain

$$\begin{aligned}
\mathrm{e}^{\beta Q(z)} &\approx \mathrm{e}^{\beta(\lambda_1+\lambda_4+Q_0)} \int_{-\infty}^{+\infty} \mathrm{d}w \mathrm{e}^{-\beta U(w)} [1-\beta V(z-w)] \\
&= \mathrm{e}^{\beta(\lambda_1+\lambda_4+Q_0)} \left[\int_{-\infty}^{+\infty} \mathrm{d}w \mathrm{e}^{-\beta U(w)}\right] [1-\beta\langle V(z-w)\rangle_{\mathrm{at}}] \\
&\approx \mathrm{e}^{\beta(\lambda_1+\lambda_4+Q_0)} \left[\int_{-\infty}^{+\infty} \mathrm{d}w \mathrm{e}^{-\beta U(w)}\right] \mathrm{e}^{-\beta\langle V(z-w)\rangle_{\mathrm{at}}}.
\end{aligned} \tag{A2}$$

Here,

$$\langle V(z-w)\rangle_{\mathrm{at}} \equiv \frac{\int_{-\infty}^{+\infty} \mathrm{d}w \mathrm{e}^{-\beta U(w)} V(z-w)}{\int_{-\infty}^{+\infty} \mathrm{d}w \mathrm{e}^{-\beta U(w)}} \tag{A3}$$

is the average of $V(z-w)$ in the atomic limit. Inserting Eq. (A2) into Eqs. (29) and (31), one then gets the high temperature asymptotic form for $\rho^{(1)}(z)$ as

$$\rho^{(1)}(z, T\to\infty) = c\,\mathrm{e}^{-\beta[U(z)+2\langle V(z-w)\rangle_{\mathrm{at}}]}. \tag{A4}$$

Using $V(z-w) = (1/2)(z-w)^2$, one obtains

$$\rho^{(1)}(z, T\to\infty) = \rho^{(1)}(0)\,\mathrm{e}^{-\beta\left(\frac{1}{n}|z|^n+z^2\right)}. \tag{A5}$$

Using the sum rule $\int_{-\infty}^{+\infty} \rho^{(1)}(z)\mathrm{d}z = 1$, we obtain

$$\begin{aligned}
1 &= \rho^{(1)}(0) \int_{-\infty}^{+\infty} \mathrm{d}z \mathrm{e}^{-\beta\left(\frac{1}{n}|z|^n+z^2\right)} \\
&\approx \rho^{(1)}(0) \int_{-\infty}^{+\infty} \mathrm{d}z \mathrm{e}^{-\beta\left(\frac{1}{n}|z|^n\right)} \\
&= \rho^{(1)}(0) 2n^{\frac{1-n}{n}} T^{\frac{1}{n}} \Gamma\left(\frac{1}{n}\right).
\end{aligned} \tag{A6}$$

This gives Eq. (49) in the main text,

$$\rho^{(1)}(z, T\to\infty) = \rho_0 T^{-\frac{1}{n}} \mathrm{e}^{-\frac{1}{T}\left(\frac{1}{n}|z|^n+z^2\right)}, \tag{A7}$$

with $\rho_0 \approx 1/\left[2n^{(1-n)/n}\Gamma(1/n)\right]$.

To derive the high temperature asymptotic expression for the correlation function, we also expand the LRT equations Eqs. (41) and (42) to leading order of $\beta V(z-w)$. We obtain

$$F(w,z) \approx \mathrm{e}^{-\beta Q(z)} \mathrm{e}^{\beta\lambda_2(w)} [1-\beta V(w-z)]. \tag{A8}$$

Inserting it into the expression for $\chi_{2k}(z)$ in Eq. (41) and employing the symmetry properties $\lambda_2(-w) = \lambda_2(w)$, $Q(-z) = Q(z)$, and $\chi_{2k}(-z) = -\chi_{2k}(z)$, we solve the equations for $\chi_{2k}(z)$ as

$$\chi_{2k}(z) \approx B(z) + \beta\,\mathrm{e}^{-\mathrm{i}k} m_k z \mathrm{e}^{-\beta Q(z)}. \tag{A9}$$

Here, m_k is given by

$$m_k \equiv \frac{\int_{-\infty}^{+\infty} \mathrm{d}z B(z) z \mathrm{e}^{\beta\lambda_2(z)}}{1-\beta\,\mathrm{e}^{-\mathrm{i}k}\int_{-\infty}^{+\infty} \mathrm{d}z z^2 \mathrm{e}^{\beta[\lambda_2(z)-Q(z)]}}. \tag{A10}$$

Inserting Eqs. (A9) and (A10) into Eq. (44) and evaluating the integral in the high temperature limit, i.e., the atomic limit $\beta V(z-w) \approx 0$ with $Q(z) \approx Q_0$, we obtain the asymptotic expression for $C(k)$,

$$\begin{aligned}
C(k)(T\to\infty) &\approx \langle z^2\rangle_{\mathrm{at}} + 2\beta\langle z^2\rangle_{\mathrm{at}}^2 f_k \\
&\approx \frac{\langle z^2\rangle_{\mathrm{at}}}{1-2\beta f_k\langle z^2\rangle_{\mathrm{at}}},
\end{aligned} \tag{A11}$$

with f_k given by

$$f_k = \mathrm{Re}\left[\frac{\mathrm{e}^{\mathrm{i}k}}{1-\beta\langle z^2\rangle_{\mathrm{at}}\mathrm{e}^{\mathrm{i}k}}\right]. \tag{A12}$$

In the derivation, $\chi_{3k}(z) = \chi_{2k}^*(z)$ has been used.

In the above equations, $\langle z^2\rangle_{\mathrm{at}} \equiv \int \mathrm{d}z z^2 \mathrm{e}^{-\beta U(z)} / \int \mathrm{d}z \mathrm{e}^{-\beta U(z)}$ can be calculated as

$$\langle z^2\rangle_{\mathrm{at}} = (nT)^{2/n} \frac{\Gamma(3/n)}{\Gamma(1/n)}. \tag{A13}$$

For $n > 2$, we take the limit $T\to\infty$ and reduce $f_k \approx \cos k$. So we obtain the high temperature expression of $C(k)$ for $n > 2$ as

$$C(k)(T\to\infty) \approx \frac{\langle z^2\rangle_{\mathrm{at}}}{1-2\beta\langle z^2\rangle_{\mathrm{at}}\cos k}. \tag{A14}$$

Now in order to extract the correlation length from the above expression, let us suppose that C_{1j} on the periodic chain has the following form:

$$C_{1j}^{\mathrm{fit}} = C_0\left(\mathrm{e}^{-\frac{j-1}{\xi}} + \mathrm{e}^{-\frac{L+1-j}{\xi}}\right), \quad (1 \le j \le L). \tag{A15}$$

Its Fourier transformation gives

$$C^{\rm fit}(k)=\sum_{j=1}^{L}C_{1j}^{\rm fit}\,{\rm e}^{{\rm i}k(j-1)}=C_0\frac{\sinh(1/\xi)}{\cosh(1/\xi)-\cos k}. \quad \text{(A16)}$$

Now we compare Eq. (A14) with Eq. (A16). Taking the limit $T\to\infty$, which implies $\xi\to 0$, we obtain the high temperature asymptotic expression $\xi(T\to\infty)$ for $n>2$, i.e., Eqs. (62) and (63) in the main text.

Appendix B: Analysis of PTA-B_1 solution

In this appendix, we analyze the PTA-B_1 results in the low and high temperature limits. Our starting point is the self-consistent equation (71). First, in the low temperature limit, $\langle x^2\rangle$ tends to zero and the summation in Eq. (71) will be dominated by the $k\to 0$ contribution where $\omega_0^2(k)=2K[1-\cos(k)]\approx Kk^2$. In the large L limit, we therefore obtain the approximate expression

$$\begin{aligned}\langle x^2\rangle_{\rm PTA}(T\to 0)&\approx\frac{T}{2\pi K}\int_0^{2\pi}{\rm d}k\frac{1}{k^2+\lambda^2}\\&\approx\frac{T}{4K\lambda},\end{aligned} \quad \text{(B1)}$$

with $\lambda^2=(n-1)!!(\gamma/K)\langle x^2\rangle^{n/2-1}$. This equation gives the low temperature expression for $\langle x^2\rangle$ as

$$\langle x^2\rangle_{\rm PTA}(T\to 0)=aT^{\frac{4}{n+2}}. \quad \text{(B2)}$$

Here $a=[16K\gamma(n-1)!!]^{-2/(n+2)}$. Using $\langle x^m\rangle\approx(m-1)!!\langle x^2\rangle^{m/2}$, we obtain Eq. (72) in the main text. The correlation function in Eq. (68) is simplified similarly in the low T limit as

$$C(k)_{\rm PTA}(T\to 0)\approx\frac{1}{\beta K}\frac{1}{k^2+\lambda^2}. \quad \text{(B3)}$$

Comparing this expression with the fitting formula (A16) in Appensix A in the $k\to 0$ limit, one obtains

$$\xi_{\rm PTA}(T\to 0)\approx\frac{1}{\lambda}=bT^{-\frac{n-2}{n+2}}, \quad \text{(B4)}$$

with $b=4K[16(n-1)!!K\gamma]^{-2/(n+2)}$.

In the high temperature limit, $\langle x^2\rangle$ tends to infinity and the summation in Eq. (71) will be dominated by the λ^2 term. We then have

$$\langle x^2\rangle_{\rm PTA}(T\to\infty)\approx\frac{T}{(n-1)!!\gamma\langle x^2\rangle^{n/2-1}}, \quad \text{(B5)}$$

which, together with $\langle x^m\rangle=(m-1)!!\langle x^2\rangle^{m/2}$ (m even), gives the asymptotic expression

$$\langle x^m\rangle_{\rm PTA}(T\to\infty)=cT^{\frac{m}{n}}, \quad \text{(B6)}$$

with $c=(m-1)!![(n-1)!!\gamma]^{-m/n}$.

Comparing the correlation function $\langle Q_k^*Q_k\rangle$ in Eq. (67) with the fitting expression Eq. (A16) and using Eq. (B6), one obtains

$$\xi_{\rm PTA}(T\to\infty)=\frac{1}{a_n^{\rm PTA}\ln T+b_n^{\rm PTA}}, \quad \text{(B7)}$$

with $a_n^{\rm PTA}=1-2/n$ and $b_n^{\rm PTA}=(2/n)\ln[(n-1)!!\gamma]-\ln K$. We find that $a_n^{\rm PTA}$ is identical to the exact value from CVM, while $b_n^{\rm PTA}$ is different from the CVM expression in Eq. (63).

Acknowledgment

Project supported by the National Natural Science Foundation of China (Grant No. 11974420).

References

[1] Lepri S 2016 *Thermal Transport in Low Dimensions: from Statistical Physics to Nanoscale Heat Transfer* (Cham: Springer)
[2] Niss K and Hecksher T 2018 *J. Chem. Phys.* **149** 230901
[3] Arceri F, Landes F P, Berthier L and Biroli G 2020 arXiv:2006.09725 [cond-mat.stat-mech]
[4] Debenedetti P G and Stillinger F H 2001 *Nature* **410** 259
[5] Ise N 1986 *Angew. Chem. Int. Ed. Engl.* **25** 323
[6] Gebbie M A, Valtiner M, Banquy X, Fox E T, Henderson W A and Israelachvili J N 2013 *Proc. Natl. Acad. Sci. USA* **110** 9674
[7] Bloomfield V A 1996 *Curr. Opin. Struct. Biol.* **6** 334
[8] Ubbink J and Odijk T 1995 *Biophys. J.* **68** 54
[9] Metropolis N and Ulam S 1949 *J. Amer. Statist. Assoc.* **44** 335
[10] Fermi E, Pasta P, Ulam S and Tsingou M 1955 *Studies of the Nonlinear Problems* (New Mexico: Los Alamos Scientific Laboratory)
[11] Alder B J and Wainwright T E 1959 *J. Chem. Phys.* **31** 459
[12] Netz R R and Orland H 2003 *Eur. Phys. J. E* **11** 301
[13] Liu J, Li B and Wu C 2016 *Europhys. Lett.* **114** 40002
[14] Liu J, Liu S, Li N, Li B and Wu C 2015 *Phys. Rev. E* **91** 042910
[15] Wu J and Cao J 2005 *Phys. Rev. Lett.* **95** 078301
[16] Szamel G 2013 *Prog. Theor. Exp. Phys.* **2013** 012J01
[17] Xu Y, Wang J S, Duan W, Gu B L and Li B 2008 *Phys. Rev. B* **78** 224303
[18] Ma K H, Guo Y J, Wang L and Tong N H 2022 *Phys. Rev. E* **106** 014110
[19] Jia H W, Liu W J, Wu Y H, Ma K H, Wang L and Tong N H 2025 *Phys. Rev. B* **111** 045153
[20] Li N and Li B 2013 *Phys. Rev. E* **87** 042125
[21] Parisi G 1997 *Europhys. Lett.* **40** 357
[22] Boyanovsky D, Destri C and de Vega H J 2004 *Phys. Rev. D* **69** 045003
[23] Aoki K and Kusnezov D 2000 *Phys. Lett. A* **265** 250
[24] Kikuchi R 1951 *Phys. Rev.* **81** 988
[25] Kubo R 1957 *J. Phys. Soc. Jpn.* **12** 570
[26] Pelizzola A 2000 *Nucl. Phys. B* **83–84** 706
[27] Pelizzola A 2005 *J. Stat. Mech.* **2005** P11010
[28] Pelizzola A 2005 *J. Phys. A: Math. Gen.* **38** R309
[29] Peierls R E 1938 *Phys. Rev.* **54** 918
[30] For a review, see Kuzemsky A L 2015 *Int. J. Mod. Phys. B* **29** 1530010
[31] Feynman R P 1972 *Statistical Mechanics* (New York: W. A. Benjamin Inc.)
[32] Morita T 1957 *J. Phys. Soc. Jpn.* **12** 753
[33] Morita T 1957 *J. Phys. Soc. Jpn.* **12** 1060
[34] An G 1988 *J. Stat. Phys.* **52** 727
[35] Morita T 1990 *J. Stat. Phys.* **59** 819
[36] Brascamp H J 1971 *Commun. Math. Phys.* **21** 56
[37] Percus J K 1977 *J. Stat. Phys.* **16** 299
[38] Kikuchi R and Beldjenna A 1992 *Physica A* **182** 617
[39] Kikuchi R 1998 *J. Phase Equilib.* **19** 412
[40] Kikuchi R 1999 *J. Stat. Phys.* **95** 1323
[41] Ren Y Z, Tong N H and Xie X C 2014 *J. Phys.: Condens. Matter* **26** 115601

[42] Yamamoto D 2009 *Phys. Rev. B* **79** 144427

[43] Kikuchi R 1951 *J. Chem. Phys.* **19** 1230

[44] Ng W M and Barry J H 1978 *Phys. Rev. B* **17** 3675

[45] Cirillo E N M, Gonnella G, Troccoli M and Maritan A 1999 *J. Stat. Phys.* **94** 67

[46] Guerrero A I, Stariolo D A and Almarza N G 2015 *Phys. Rev. E* **91** 052123

[47] Guerrero A I, Stariolo D A 2017 *Physica A* **466** 596

[48] Kikuchi R 1974 *J. Chem. Phys.* **60** 1071

[49] McCormack R, Asta M, de Fontaine D, Garbulsky G and Ceder G 1993 *Phys. Rev. B* **48** 6767

[50] Sanchez J M, Ducastelle F and Gratias D 1984 *Physica A* **128** 334

[51] Morita T and Tanaka T 1966 *Phys. Rev.* **145** 288

[52] Tanaka T and Libelo L F 1975 *Phys. Rev. B* **12** 1790

[53] Halow J, Tanaka T and Morita T 1968 *Phys. Rev.* **175** 680

[54] Morita T 1994 *Prog. Theor. Phys.* **92** 1081

[55] Tanaka T, Hirose K and Kurati K 1994 *Prog. Theor. Phys. Suppl. No.* **115** 41

[56] Finel A 1994 *Suppl. Prog. Theor. Phys.* **115** 59

[57] Mohri T 2013 *JOM* **65** 1510

[58] Tanaka K 2003 *IEICE Trans. on Information and Systems* **E86-D** 1228

[59] Tanaka K 2005 *International Conference on Computational Intelligence for Modelling, Control and Automation and International Conference on Intelligent Agents, Web Technologies and Internet Commerce (CIMCA-IAWTIC'06)* November 28–30, 2005, Vienna, Austria, pp. 669–675

[60] Das A 2008 *Lectures on Quantum Field Theory* (Hackensack, USA: World Scientific)

[61] Dmitriev S V, Kevrekidis P G and Yoshikawa N 2006 *J. Phys. A: Math. Gen.* **39** 7217

[62] Xu L and Wang L 2016 *Phys. Rev. E* **94** 030101

[63] Liu Y and He D 2021 *Chin. Phys. Lett.* **38** 044401

[64] Yang L, Li N and Li B 2014 *Phys. Rev. E* **90** 062122

[65] Aoki K and Kusnezov D 2001 *Phys. Rev. Lett.* **86** 4029

[66] Gillan M J 1984 *J. Phys. C: Solid State Phys.* **17** L237

[67] Casati G, Ford J, Vavaldi F and Visscher W M 1984 *Phys. Rev. Lett.* **52** 1861

[68] Onodera Y 1970 *Prog. Theor. Phys.* **44** 1477

[69] Toda M 1967 *J. Phys. Soc. Jpn.* **22** 431

[70] Toda M 1967 *J. Phys. Soc. Jpn.* **23** 501

[71] Mareschal M and Amellal A 1988 *Phys. Rev. A* **37** 2189

[72] Morán-López J L and Sanchez J M 1996 *Theory and Applications of the Cluster Variational and Path Probability Methods* (New York and London: Plenum Press)